Copy No. _____

Defence Research and Development Canada
Recherche et développement pour la défense Canada

DEFENCE DÉFENSE

Metal Oxide Materials and Collector Efficiency in Electrochemical Supercapacitors

Final Report

Tarik Bordjiba
Gwenaël Chamoulaud
Christelle Médard
Maude Hélène Lechasseur
Daniel Bélanger
Université du Québec à Montréal

Prepared by:
Université du Québec à Montréal
Département de Chimie
Case postale 8888, Succ. Centre-ville
Montréal (Québec) H3C 3P8

Project Manager: Daniel Bélanger, 514-987-3000 ext. 3909
Contract Number: W7707-063348
Contract Scientific Authority: Colin G. Cameron, 902-427-1367

Defence R&D Canada – Atlantic

Contract Report
DRDC Atlantic CR 2010-255
December 2010

Canada

This page intentionally left blank.

Metal Oxide Materials and Collector Efficiency in Electrochemical Supercapacitors

Final Report

Tarik Bordjiba
Gwenaël Chamoulaud
Christelle Médard
Maude Hélène Lechasseur
Daniel Bélanger
Université du Québec à Montréal

Prepared by:

Université du Québec à Montréal
Département de Chimie
Case postale 8888, Succ. Centre-ville
Montréal (Québec) H3C 3P8

Project Manager: Daniel Bélanger 987-3000 ext. 3909
Contract Number: W7707-063348
Contract Scientific Authority: Colin G. Cameron 902-427-1367

Defence R&D Canada – Atlantic
Contract Report
DRDC Atlantic CR 2010-255
December 2010

Approved by

Original signed by Leon Cheng

Leon Cheng
Head/Dockyard Laboratory (Atlantic)

Approved for release by

Original signed by Ron Kuwahara for

Calvin Hyatt
Chair/Document Review Panel

Abstract

The Supercapacitor Technology Investment Fund (TIF) project aimed to develop improved supercapacitor performance through the design of better electrode materials. This will ultimately yield devices with elevated power and energy densities and/or performance tailored to the needs of the Canadian military. This report deals with the development of electrochemical supercapacitors based on MnO_2 and binary manganese and ruthenium oxides with the use of various current collectors. The binary oxides were prepared and characterized by physicochemical and electrochemical techniques. The effect of the heat-treatment on the capacitance of the binary oxides was investigated as well as the effect of the supporting electrolyte, the current collector and the composition of the composite electrode. Carbon nanotubes were coated on a carbon paper and used as support for the binderless spontaneous formation of MnO_2. A correlation is drawn between pore size and capacitor performance for the combinations of active material, binder, and conductive carbon. New results are presented along with a summary of results from the previous two years of the project, and the performance of these new electrode materials is highlighted.

Résumé

Le projet de «fonds d'investissement en technologie» (FIT) sur les supercapacités visait à améliorer la performance des supercapacités par créer de meilleurs matériaux pour les électrodes. Ceci produira enfin des dispositifs possédant des niveaux élevés d'énergie et de puissance, et/ou personnalisés pour les besoins des forces canadiennes. Ce rapport traite du développement de supercapacités électrochimiques basées sur des oxydes de manganèse et des oxydes binaires RuO_2/MnO_2 et utilisant divers collecteurs de courant. Les oxydes binaires ont été préparés et caractérisés selon de diverses méthodes physicochimiques et électrochimiques. L'effet du traitement thermique sur la capacité des oxydes binaires a été étudié ainsi que l'effet de la nature de l'électrolyte support, du collecteur de courant et de la composition de l'électrode composite. Un collecteur de courant obtenu par la déposition de nanotubes de carbone sur un papier carbone a été utilisé comme substrat pour la déposition spontanée de MnO_2 sans liant. On dévoile une corrélation entre la taille des pores et la performance des supercapacités for les divers combinaisons de matériau actif, liant, at carbone conducteur. Les nouveaux résultats sont présentés ainsi qu'un résumé des résultats des deux années précédentes du programme, et la performance de ces nouveaux matériaux est soulignée.

This page intentionally left blank.

Executive summary

Metal Oxide Materials and Collector Efficiency in Electrochemical Supercapacitors: Final Report

Tarik Bordjiba, Gwenaël Chamoulaud, Christelle Médard, Maude Hélène Lechasseur, Daniel Bélanger; DRDC Atlantic CR 2010-255; Defence R&D Canada – Atlantic; December 2010.

Background: The Supercapacitor Technology Investment Fund (TIF) project aimed to develop improved supercapacitor technology through the design of better electrode materials. This will ultimately yield devices with elevated power and energy densities and/or performance tailored to the needs of the Canadian military. The present work focused on optimizing electrode materials based on manganese oxide, an inexpensive and relatively benign material with promising energy storage properties.

Principal Results: This research was conducted by Daniel Bélanger at Université du Québec à Montréal. A number of key results arose over the course of the three year project: (i) chemical modifications to the titanium current collector led to enhanced conductivity across the interface, (ii) mixed oxides of ruthenium and manganese showed promise, but a co-precipitated compound was not significantly better than a simple mechanical mixture, (iii) binder-free manganese dioxide–carbon nanotube composites can be deposited spontaneously on carbon substrates, (iv) thin film mixed oxide systems showed promising power densities, especially in acidic media, and (v) a study of the loadings of manganese oxide, carbon filler, and Nafion binding showed a correlation between porosity and capacitance, and concluded that the addition of the ionic conductor Nafion is in fact detrimental to the cell performance.

Significance: The increased reliance on electronic equipment in modern warfare necessitates a parallel development of electrical power systems. Supercapacitors, having properties somewhere between a battery and a conventional capacitor, fill an important need; certain technologies (e.g., radio transmitters, sensors, and future weapons) demand large pulses of power. Better materials will lead to better capacitors, which in turn will lead to better tools for the military. The present work produced materials with performance superior to those used currently in commercial off-the-shelf supercapacitors.

Future Work: This TIF project has now ended. Follow-on work is underway, both to carry the lab-scale results from the program to a prototype, as well as producing proof-of-concept devices that illustrate supercapacitors for pulse power in applications relevant to the Canadian Forces.

Sommaire

Metal Oxide Materials and Collector Efficiency in Electrochemical Supercapacitors: Final Report

Tarik Bordjiba, Gwenaël Chamoulaud, Christelle Médard, Maude Hélène Lechasseur, Daniel Bélanger ; DRDC Atlantic CR 2010-255 ; R & D pour la défense Canada – Atlantique ; décembre 2010.

Contexte : Le projet de «fonds d'investissement en technologie» (FIT) sur les supercapacités visait à améliorer la performance des supercapacités par créer de meilleurs matériaux pour les électrodes. Ceci produira enfin des dispositifs ayant des niveaux élevés d'énergie et de puissance, et/ou personnalisés pour les besoins des forces canadiennes. Ce rapport traite de l'optimisation des matériaux basés sur l'oxyde de manganèse, un matériau inoffensif et peu coûteux qui possède des propriétés prometteuses pour le stockage d'énergie.

Résultats principaux : Ce projet de recherches a été mené par Daniel Bélanger à l'Université du Québec à Montréal. De nombreux résultats se sont dévoilés au cours du projet qui a duré trois ans : (i) des modifications chimiques du collecteur de courant en titanium ont produit une conductivité élevée à travers l'interface, (ii) les oxydes combinés de ruthénium et manganèse étaient prometteurs, mais le composé co-précipité n'était pas meilleur qu'un mélange simple, (iii) on peut déposer sur un substrat de carbone des composites sans liant de dioxyde de manganèse et des nanotubes de carbone, (iv) les systèmes d'oxydes combinés en couches minces démontrent de bonnes densités de puissance, surtout dans des médias acidiques, et (v) une étude du chargement de l'oxyde de manganèse, la charge de carbone, et le liant Nafion a démontré un lien entre la porosité et capcité et que le conducteur ionique Nafion était justement délétère pour la performance du dispositif.

Portée : L'équipement dont se servent les armées modernes dépend de plus en plus de l'énergie électrique, exigeant le développement de nouveaux systèmes d'alimentation. En tant que dispositif en partie batterie et en partie condensateur conventionnel, les supercapacités fournissent d'énergie pulsée pour les technologies qui en ont besoin, tel que les transmetteurs, les capteurs, et les armes futures. Des meilleurs matériaux mèneront à des supercapacités supérieures qui permettront des outils supérieures pour les forces canadiennes. Les résultats ont indiqué que les matériaux qu'on a étudiés démontrent une performance améliorée par rapport aux supercapacités commerciales disponibles à date.

Recherches futures : Ce projet FIT est maintenant fini. Des recherches suivantes sont en cours, par exemple, on essaie d'augmenter réaliser un prototype en utilisant les matériaux qu'on a découvert. De plus on est en train de fabriquer des démonstrations du bien-fondé de la conception de l'exploitation afin d'élaborer les supercapacités et la puissance pulsée dans des applications visées aux forces canadiennes.

This page intentionally left blank.

Table of contents

List of figures

List of tables

1 Introduction

An electrochemical capacitor is a charge storage device with characteristics between a conventional electrostatic capacitor and a rechargeable battery [1]. It has various applications particularly in the fields of electrical equipment and hybrid electric vehicles [2]. An electrochemical capacitor consists of two electrodes, an electrolyte and a separator. The performance (energy and power densities) and the durability of the electrochemical capacitors depend greatly on the electrode material. An electrochemical capacitor electrode consists of at least two components: the active electrode material and the current collector. One of the major goals of the research and development in the field of energy storage is the synthesis of active electrode materials with high performance and stability over cycling. A less-examined point is the integration of the active material with the current collector without loss of performance or stability and while maintaining a low resistivity.

The objectives of this part of the project have been: (i) improve the interfacial characteristics between the active electrode material and the current collector, and (ii) develop new oxides (active materials) for electrochemical capacitors.

In order to improve the interfacial characteristics between the active electrode material and the current collector, two approaches were used (Figure 1): (i) formation of titanium oxides nanotubes, and (ii) deposition of carbon nanotubes on a conducting substrate. For the development of new oxides, this group has synthesized (Figure 2): (i) mixed oxides of RuO_2/MnO_2, and (ii) nanocomposites based on carbon nanotubes and manganese oxide.

2 Improving the interfacial characteristics between the active electrode material and the current collector

An important parameter in the development of electrochemical supercapacitors is the equivalent series resistance (ESR). Because of the high currents developed by capacitors, the ESR can lead to very significant voltage drops, and hence severely limit the power density that can be delivered. Thus, it is of the utmost importance to maintain a low ESR. A major contribution to the ESR originates from the electrical contact between the active electrode material and the current collector. Furthermore, an increase of the ESR is often observed during prolonged charge/discharge cycling. In order to improve interfacial characteristics between the active electrode material and the current collector two different approaches were proposed: (i) formation of titanium oxide nanotubes, (ii) deposition of carbon nanotubes (CNTs) on a conducting substrate.

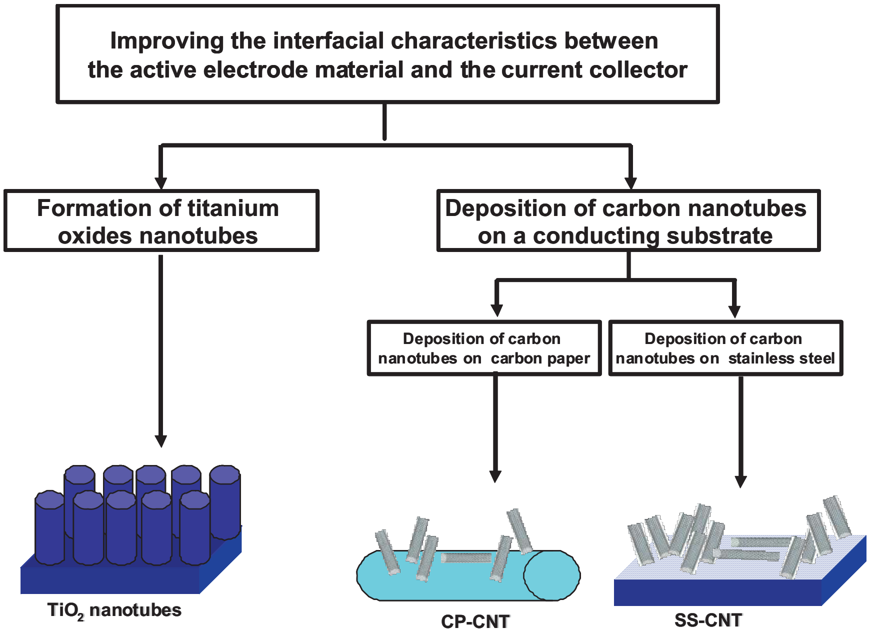

Figure 1: *Strategy to improve the interfacial characteristics between the active electrode material and the current collector.*

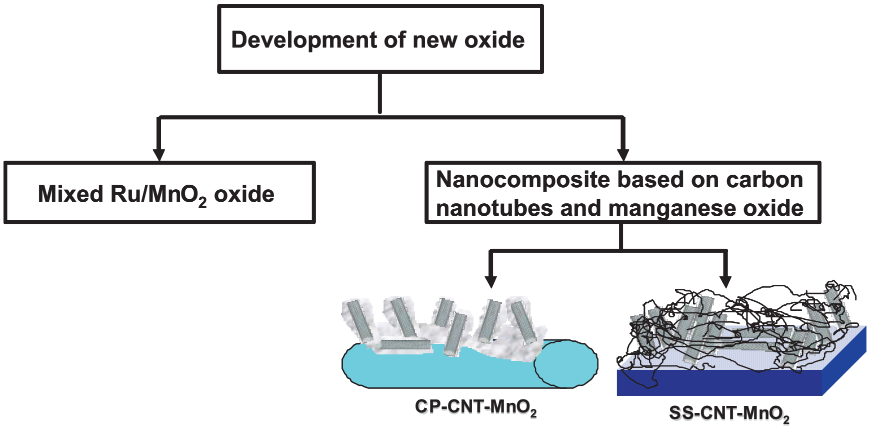

Figure 2: *Strategy for the development of new oxides.*

2.1 Development of titanium oxide nanotubes

Highly nanostructured titania layers can be obtained using oxidative treatments. For example, amorphous TiO_x nanofibres can be fabricated by impregnating a mesoporous silica film with $TiCl_4$ that is then hydrolyzed in air [3]. Titania nanorods [4] and titania nanoflowers [5] have been synthesised through the direct oxidation of titanium with hydrogen peroxide at low temperature. Titanium oxide nanotubes were also obtained by successive NaOH and HCl chemical treatments [6, 7], anodic oxidation in HF [8] or in $NH_4HF_2/NH_4H_2PO_4$ [9] aqueous solutions, and also by sonochemical synthesis [10]. However, even if thick titanium films and/or nanostructured layers were obtained using these methods, they were composed of non-conducting titanium oxides, rendering them less interesting for current collector applications.

A review of the literature suggests that deposition of thick layers of pure titanium metal is not easy to achieve. On the other hand, nanostructured titanium electrodes with high surface roughness could be obtained by chemical or electrochemical methods with reductive or oxidative treatments. Unfortunately, those electrodes were mostly composed of passivated titanium oxides instead of conductive titanium metal. However, is has been shown that it is possible to decrease the thickness of the TiO_2 layer electrochemically and hence increase its conductivity.

2.1.1 Synthesis of titanium oxide nanotubes

The titanium oxide nanotubes were prepared with the following procedure:

1. Polishing the as-received titanium electrode.
2. Electrochemical modification of electrode. Titanium electrodes were modified by potentiostatic polarisation at +20 V for 6 h in aqueous $NH_4HF_2/NH_4H_2PO_4$ solution.
3. Electrochemical reduction treatment in $LiClO_4$/acetonitrile.

2.1.2 Characterization of titanium oxide nanotubes

Figure 3 presents scanning electron microscope (SEM) images of titanium oxide nanotubes, both as-formed and following electrochemical reduction in $LiClO_4$/acetonitrile. Table 1 reports the electrochemical parameters and the atomic composition of the titanium electrode following various treatments. After potentiostatic polarization at $+20$ V, a tube-like structure is formed at the titanium electrode surface (Figure 3a). These nanotubes have an internal diameter of around 100 nm and an estimated length of between 300 and 400 nm (Figure 3d). A proposed mechanism for the formation of these anodically-formed nanotubes is the migration of titanium ions from the interpore areas of the oxide film to the oxide/solution interface [8]. At high anodization voltages, the electric field is strong enough

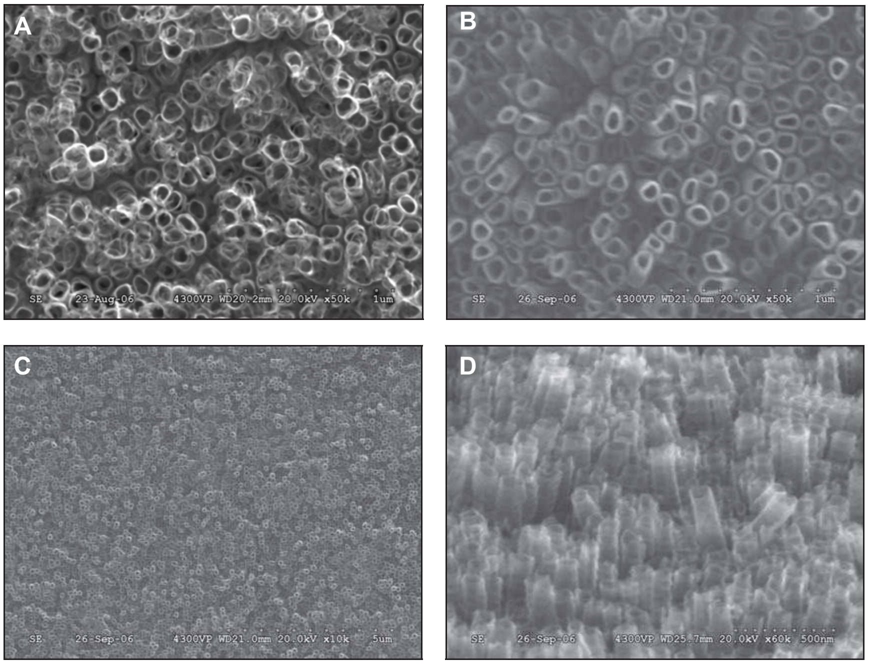

Figure 3: *SEM images of titanium electrodes modified by potentiostatic polarisation at* $+20$ *V for 6 h in aqueous* $NH_4HF_2/NH_4H_2PO_4$ *solution: (a) 50,000× magnification and after electrochemical reduction treatment in* $LiClO_4$*/acetonitrile, (b) 50,000× magnification, (c) 10,000× magnification, and (d) 60,000× magnification at an angle of 45°.*

to move these ions, and their migration leaves voids in the interpore areas, eventually separating the pores and forming discrete tube-like structures. After the electrochemical reduction in $LiClO_4$/acetonitrile, the structure of the nanotubes seems better defined (Figure 3b). This is attributed to the higher conductivity of the electrode which improves the SEM focus. It should also be noted that during the electroreduction in $LiClO_4$/acetonitrile media, the electrode changed colour, from shiny grey/gold to opaque black. Finally, at lower magnification (Figure 3c), the structure of the titanium oxide nanotubes appears homogeneous.

After anodization the open-circuit potential (OCP) the resistance was higher than that of a freshly polished titanium electrode (Table 1). After electrochemical reduction in $LiClO_4$/ acetonitrile, the resistance was lower than that of a polished titanium electrode. As previously observed with a H_2O_2 treatment, the lower resistance comparable to that of the polished electrode could be due to the increase of the electrode specific surface area [11]. Before electrochemical reduction, the O:Ti ratio was about 1; the modified electrode surface was mostly composed of the TiO species. After electrochemical reduction, this ratio increased to 1.5, and this higher ratio could be explained by the formation of the Ti_2O_3 species, which is highly conductive). The oxidation of a fraction of the TiO oxide to TiO_2 (highly resistive) is thermodynamically unlikely. Moreover, the observed opaque black colour for the electrode after reduction in $LiClO_4$/acetonitrile media confirms the forma-

Table 1: *Open circuit potential, resistance and O:Ti atomic ratio for a titanium electrode modified by potentiostatic polarization at* $+20$ *V for 6 h in aqueous* $NH_4HF_2/NH_4H_2PO_4$ *solution, before and after the electrochemical reduction treatment in* $LiClO_4$*/acetonitrile.*

Electrode	OCP V *vs*. Ag/AgCl	Resistivity $\Omega\cdot cm^2$	O:Ti atom ratio
Polished	−0.230	2103	0.33
After anodization	+0.405	4419	1.13
After reduction	−0.113	803	1.49

tion of Ti_2O_3 species, which has a dark blue colour. However the exact mechanism of the Ti_2O_3 formation remains unclear.11.0pt plus 2.0pt minus 1.0pt

The formation of titanium nanotubes by anodization in $NH_4HF_2/NH_4H_2PO_4$ led to an increase of the titanium electrode surface area, and the subsequent electrochemical reduction in acetonitrile solution increased the conductivity of the electrode without losing the nanotube-like structure. Such a structure could be useful as the current collector interface within an electrochemical capacitor.

2.2 Deposition of carbon nanotubes on conductor substrate

Recent studies have shown that a surface treatment of an Al current collector can significantly decrease its resistance [12, 13]. The surface treatment involved an etching process that is followed by coating the current collector with a carbonaceous material [12] or carbon nanofibres [13]. A non-aqueous electrolyte had been used is those studies, but in the present project, electrochemical capacitors based on aqueous electrolyte were developed, so different approaches may be necessary to minimize the resistance of the current collector/active electrode material interface.

2.2.1 Deposition of carbon nanotubes on microfibre carbon paper

Purified (90%) CNTs (multiwall, 10–15 nm o.d., 2–6 nm i.d., 0.1–10 μm length) prepared by chemical vapor deposition were purchased from Aldrich and used without further purification. All other chemicals used in this study were purchased from Aldrich and used as received. Deionized water (18 MΩ·cm, Branstead Nanopure II) was used to prepare the solutions. Carbon paper (CP) was purchased from Spectracarb (SC 2050A), and used without further treatment.

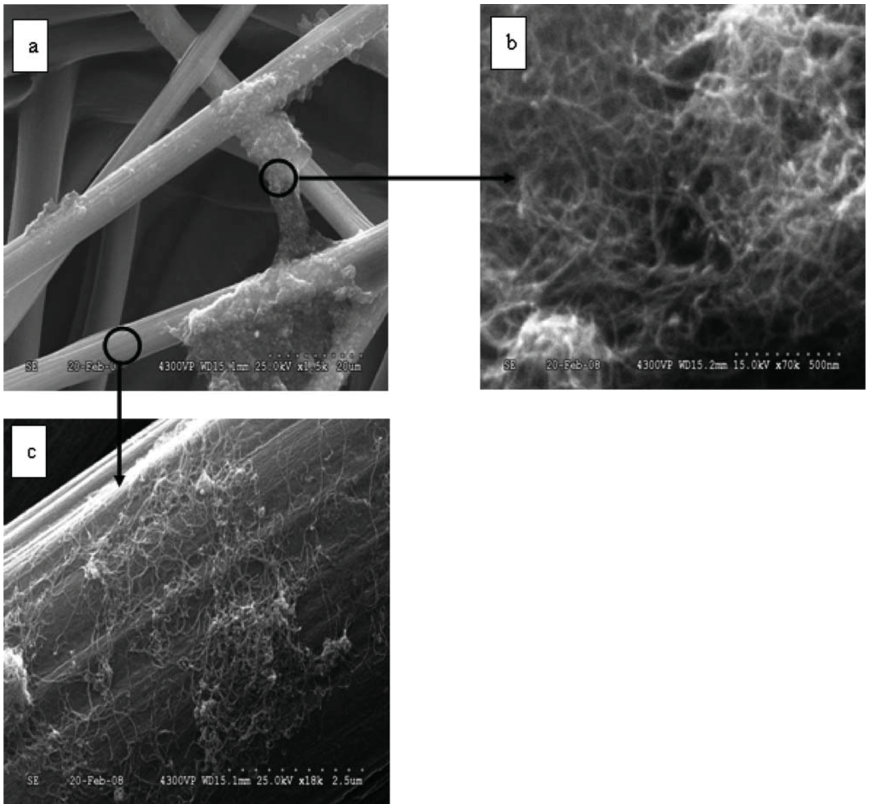

Figure 4: *SEM images of the CP-CNT nanocomposite: (a)1500×, (b) 70,000×, and (c) 18,000×.*

CNTs (100 mg) were dispersed in 100 mL of ethanol using ultrasonication (FS 30, Fisher Scientific) for 30 min, without surfactant. A sheet of CP was coated with CNTs by dip coating for 30 min. The sheet was then washed and dried under vacuum at room temperature. The resulting material is denoted CP-CNT.

Figure 4 shows an image of CP-CNT, where CNTs are deposited on the microfibrous CP, either as networks that form bridges between the CP microfibres (Figure 4b) or simply dispersed on the surface of the CP (Figure 4c). This CP-CNT nanocomposite was used as a current collector and substrate for the active material, manganese oxide.

2.2.2 Deposition of carbon nanotubes on stainless steel by electrophoresis

The CNTs described in the previous section (§2.2.1) were also used here. 304 stainless steel gauze (SS) was obtained from Alfa Aesar. To functionalize CNTs with acidic sites, 0.8 g of CNTs were refluxed in 60 mL of 1:3 (volume ratio) concentrated nitric and sulfuric acids at 130°C for 30 min [14]. Finally, the oxidized carbon nanotubes were washed with deionized water.

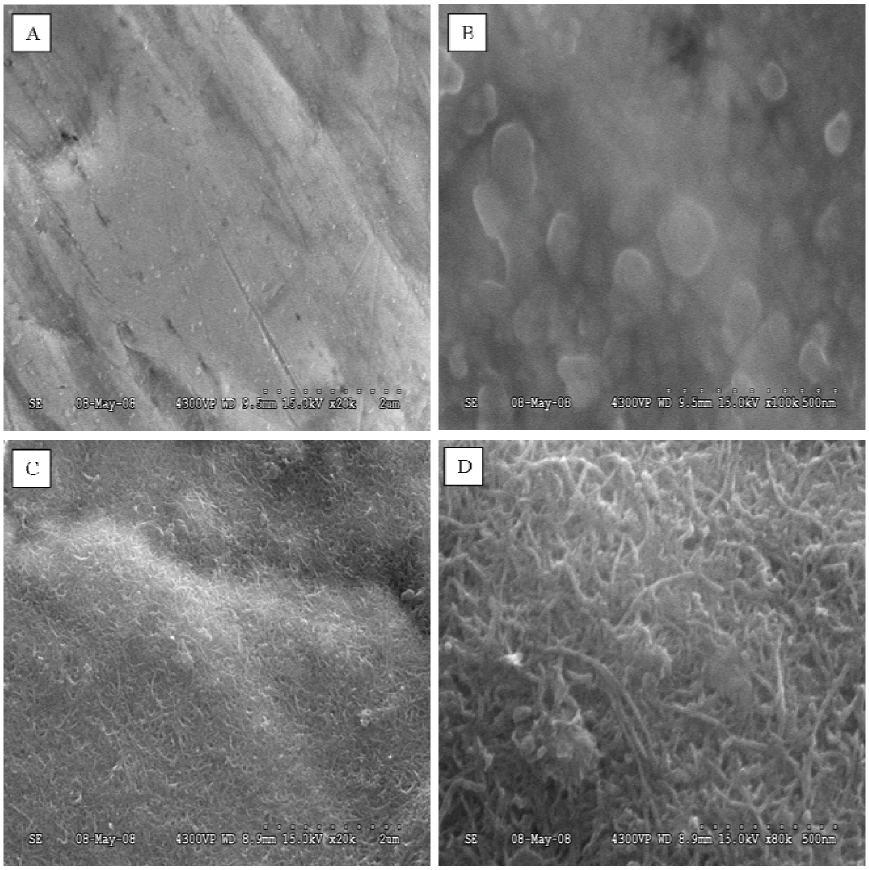

Figure 5: *SEM images of the stainless steel substrate at (a) 20,000× and (b) 100,000×, and CNTs deposited on the substrate at (c) 20,000× and (d) 80,000×.*

An aqueous suspension of the treated CNTs (0.5 mg/mL) was used for electrophoretic deposition on the SS substrate [15]. The 2 cm × 1 cm stainless steel substrate was prepared by an ultrasonic treatment in acetone for 10 min and dried under vacuum at room temperature for 24 hr. Electrophoretic deposition was conducted at constant voltage 40 V for 4 min, with an electrode separation of 2 cm. After electrophoretic deposition, the samples were dried under vacuum at room temperature for 24 hr. This sample was denoted SS-CNT.

SEM images of the various electrodes are shown in Figure 5. The stainless steel substrate presents a smooth surface (Figures 5a and 5b), whereas a rougher morphology is obtained following the electrophoretic deposition of CNTs (Figures 3c,d). The CNT film is highly porous with open space between the entangled nanotubes. Thus, the SS-CNT electrode is suitable for use as a current collector and substrate for the nanoscale manganese oxide active material.

3 Development of mixed-oxide electrodes

3.1 Development of mixed oxide RuO_2/MnO_2

Co-precipitation of $RuO_y \cdot n(H_2O)$, abbreviated hereafter as RuO_2, and MnO_2 with other metal oxides has previously been achieved in aqueous media. For instance, binary oxides such as Ni/RuO_2 [16] and MnO_2/ZnO_2 [17] have been formed by the oxidation of the corresponding salts in NaOH and NH_4^+ aqueous solutions, respectively. However, the simultaneous co-precipitation of RuO_2 and MnO_2 has not been reported until now. Such a material offers the possibility of combining the high performance of ruthenium oxides with the low cost of manganese oxides.

The acidification of a $KMnO_4$ solution is known to yield MnO_2 as a solid, whereas $RuCl_3$ precipitates as hydrated ruthenium oxide in alkaline aqueous media [18, 19]. The expected redox reactions involved in each precipitation are:

$$\begin{aligned} MnO_4 + 4H^+ + 3e^- &\longrightarrow MnO_2 + 2H_2O \qquad && E^0 = +1.679\text{ V} \\ 2Ru_3^+ + 2OH^- &\longrightarrow Ru(OH)_2^{2+} + 1e^- \qquad && E^0 = +0.86\text{ V} \end{aligned}$$

The $Ru(OH)_2^{2+}$ cations can then precipitate as various oxides, such as $RuO_2 \cdot 2H_2O$:

$$Ru(OH)_2^{2+} + 2OH^- \longrightarrow RuO_2 \cdot 2H_2O$$

The potential difference of +0.84 V between those two redox systems seems large enough to predict the following reaction between $KMnO_4$ and $RuCl_3$:

$$MnO_4^- + 3Ru^{3+} + 2H_2O + 2OH^- \longrightarrow MnO_2 + 3Ru(OH)_2^{2+}$$

Therefore, the simultaneous co-precipitation of MnO_2 and RuO_2 from MnO_4 and $RuCl_3$ should occur in aqueous media.

3.1.1 Materials synthesis

3.1.1.1 RuO_2

The RuO_2 powder was synthesized by adding 0.51 g of $RuCl_3$ to 200 mL of 1 M NaOH. The solution was then stirred for 12 hours, slowly producing a dark black precipitate [18, 19]. The precipitate was filtered (Whatman no. 54 paper filter) and washed successively with 200 mL of water, 100 mL of methanol and 100 mL of acetone. Finally, the powder was dried and stored under vacuum at 40°C until use.

3.1.1.2 MnO_2

The MnO_2 powder was synthesized according to a simple co-precipitation method [20,21]. $KMnO_4$ (99% purity) was dissolved in deionized water, and $MnSO_4$ was slowly added with stirring. The $KMnO_4$:$MnSO_4$ molar ratio was 2:3. A dark brown precipitate was immediately obtained in accordance with:

$$2\,KMnO_4 + 3\,MnSO_4 + 2\,H_2O \longrightarrow 5\,MnO_2 + 4\,H^+ + 2\,K^+ + 3\,SO_4^{2-}$$

The solution was filtered (Whatman no. 54 paper filter). The precipitate was then dispersed in deionized water and stirred for 5 min using an ultrasonic bath. The same operation was carried out twice more, first in methanol and then in acetone. The resulting powder was dried at 40°C for 12 h under vacuum.

3.1.1.3 RuO_2/MnO_2

A 10 mM $KMnO_4$ aqueous solution (25 mL) was added drop-wise to 100 mL of 1 M NaOH. The solution was stirred for ten minutes. Next, 25 mL of 10 mM $RuCl_3$ aqueous solution was added drop-wise and the mixture was stirred for 10 minutes. Finally, 100 mL of 1M HCl was added to the alkaline solution and the mixture was stirred for 12 hours. The mixture led to the formation of a precipitate. This precipitate was filtered and washed respectively with 200 mL of water, 100 mL of methanol, and 100 mL of acetone. The resulting powder was dried and stored under vacuum at 40°C until to use.

3.1.1.4 composite electrodes

The composite electrodes were prepared by mixing different quantities of active material powders (RuO_2, MnO_2, or RuO_2/MnO_2 binary oxide) with acetylene black (Alfa Aesar, $> 99.9\%$), graphite (Alfa Aesar, $> 99.8\%$) and 5% w/w of poly(tetrafluoroethylene) powder (PTFE). Table 2 shows the compositions of the prepared composite electrodes. The composite electrode components (except PTFE) were mixed with an excess of ethanol (approximately 5 mL) for five minutes in an ultrasonic bath. The PTFE was then added, and the mixture was sonicated for a further ten minutes. The excess of ethanol was allowed to evaporate under a weak vacuum at 25°C. The resulting rubber-like paste was rolled into a film on a flat glass surface. The thickness of this film was measured using a Mitutoyo Digimatic Micrometer and was $110 \pm 10\ \mu$m. A section of this film (around 2 mg) was cut and pressed under 9 tons/cm^2 on a stainless steel grid that was used as current collector. The thickness of the assembly was determined to be $268 \pm 26\mu$m.

3.1.2 Materials characterization

3.1.2.1 The effects of electrode composition

The specific capacitance values of composite electrodes ($C_{sp,E}$) determined from cyclic voltammetry (CV) are reported in Table 3. For RuO_2 composite electrodes, the specific

Table 2: *Composition of RuO_2, MnO_2, and co-precipitated RuO_2/MnO_2 composite electrodes.*

Composite Electrode	Active Material* % w/w	Acetylene Black % w/w	Graphite % w/w	PTFE % w/w
AM-60	60	17.5	17.5	5
AM-70	70	12.5	12.5	5
AM-80	80	7.5	7.5	5
AM-90	90	5.0	0.0	5

*Active materials are RuO_2, MnO_2, or RuO_2/MnO_2 binary oxides (mixture or co-preciptated)

capacitances are lower than those known for RuO_2 composite electrodes in H_2SO_4 electrolyte, approximately 700 F/g [22]. This large difference is due to the use of K_2SO_4 instead of H_2SO_4 as the electrolyte. The RuO_2 composite electrode containing 90% active material shows the highest specific capacitance (182 F/g).

The specific capacitance of the MnO_2 composite electrodes are similar to those reported in the literature for K_2SO_4 aqueous solutions [23]. The highest specific capacitances are obtained for a composition of 80% active material, 142 F/g. For a composition of 90% active material, the specific capacitance decreased. This decrease indicates that at this loading, not all the active material present in the electrode is electrochemically accessible, presumably due to the low concentration of conducting material. For a MnO_2 content lower than 70%, there is a decrease in the specific capacitance.

For binary oxide composite electrodes (RuO_2+MnO_2 and RuO_2/MnO_2) the capacitance values are of the order expected from the weighted capacitance of the individual oxides (RuO_2 and MnO_2), given their proportions in the composite electrode (1:3). The variation of the specific capacitance for the RuO_2+MnO_2 and RuO_2/MnO_2 composite electrodes is similar to that observed in the MnO_2 electrodes (Table 3), with a maximum specific capacitance corresponding to active material content. This is consistent with the observation of a maximum $C_{sp,E}$ for the MnO_2 composite electrodes having 75% active material [23].

A comparison of the RuO_2+MnO_2 and RuO_2/MnO_2 composite electrodes shows that the capacitance of binary oxide electrodes prepared by co-precipitation is slightly higher than those prepared by simple mixing. However, the difference is not great enough to conclude that these materials exhibit different performance.

Table 3 also presents the intrinsic specific capacitance of the active material alone, $C_{sp,M}$. The known contribution of acetylene black, 3.9 F/g, has been subtracted. No obvious $C_{sp,M}$ trend can be discerned from the results. An increased proportion of carbonaceous filler (from 5% in the AM-90 formulation to 35% in AM-60) ought to increase the bulk conductivity of the electrodes, and hence permit better electrochemical access to the active

Table 3: *Electrode specific capacitance ($C_{sp,E}$, F/g) and active material intrinsic specific capacitance ($C_{sp,M}$, F/g) for different compositions of RuO_2, MnO_2, RuO_2+MnO_2, and co-precipitated RuO_2/MnO_2 electrodes.*

Composite Electrode	RuO_2		MnO_2		RuO_2+MnO_2		RuO_2/MnO_2		RuO_2+MnO_2 (theo)*	
	$C_{sp,E}$	$C_{sp,M}$	$C_{sp,E}$	$C_{sp,M}$	$C_{sp,E}$	$C_{sp,M}$	$C_{sp,E}$	$C_{sp,M}$	$C_{sp,E}$	$C_{sp,M}$
AM-60	116	190	96	157	98	160	101	166	101	165
AM-70	136	193	89	125	102	144	137	195	101	142
AM-80	180	224	141	175	138	171	142	177	151	187
AM-90	182	202	116	129	131	145	140	155	132	147

* Theoretical value calculated from RuO_2 and MnO_2 specific capacitance for a binary oxide composite electrode with a Ru/Mn atomic ratio equal to 1/3.

material. One would expect an increase in material specific capacitance to correspond to a decrease in the fraction of active material. This was not observed, suggesting (i) that the electrode composition is not the primary determinant of electrode conductivity, and/or (ii) that the electrochemical access to the active material is not influenced by the bulk conductivity. However, there are useful comparisons to be made between the formulations presented in Table 3.

As expected, the highest intrinsic material specific capacitances were obtained for RuO_2 composite electrodes, over 190 F/g, with the highest value coming from the electrode containing 80% RuO_2, $C_{sp,M} = 224$ F/g. The intrinsic specific capacitance values obtained for MnO_2 composite electrodes are between 125 and 175 F/g, lower than those found for RuO_2. The $C_{sp,M}$ for binary oxide electrodes (RuO_2+MnO_2 and RuO_2/MnO_2) lie between between the capacitance of RuO_2 and MnO_2 composite electrodes. For both binary oxide electrodes, the highest capacitances were obtained with an active material loading of 80%, 171 and 177 F/g for RuO_2+MnO_2 and RuO_2/MnO_2 electrodes, respectively. As noted earlier, the intrinsic specific capacitances of binary oxide electrodes prepared by the co-precipitation are slightly higher than those prepared by simple mixing but again the difference does not appear to be significant.

The expected intrinsic specific capacitances of RuO_2+MnO_2 electrodes are of the same order as those obtained for the binary oxides electrodes prepared by simple mechanical mixing or by co-precipitation. This suggests that there is no added benefit in the simple mixtures of RuO_2 and MnO_2 materials. Nor is there an increase in the CV potential windows. The only noticeable positive effect of using co-precipitated RuO_2/MnO_2 is the yield of slightly higher capacitance values compared to those obtained from the simple mixing method.

The conclusion to be drawn is that electrodes containing 80% active material exhibit the best overall performance, and so this formulation was used in subsequent experiments.

3.1.2.2 The contributions of the current collector

The application of titanium as the current collector was described earlier (Section 2.1). It was shown that chemical and electrochemical treatments can lead to surface nanostructure. Subsequent electrochemical reduction produced a surface suitable for use as a current collector.

The RuO_2+MnO_2 composite electrode data presented earlier in the present Section were obtained with a stainless steel grid collector. Figure 6 compares the CVs of amorphous RuO_2+MnO_2 composite electrodes using either stainless steel or titanium current collectors.

The CVs are similar, indicating that the specific capacitances are essentially the same. The potential window with a titanium current collector is larger (1.05 V) than the one obtained

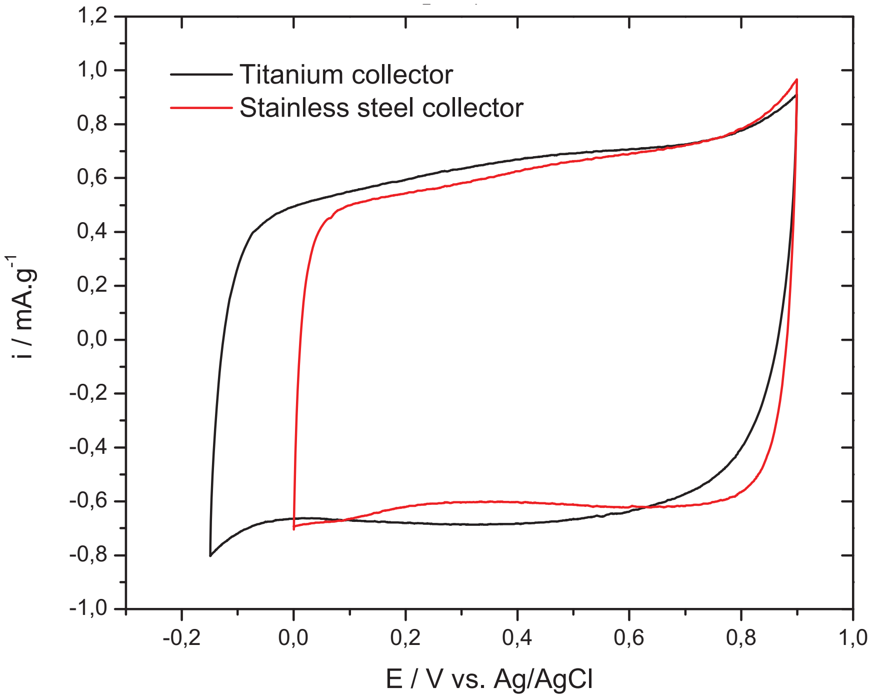

Figure 6: *Cyclic voltammograms of* RuO_2*+*MnO_2 *composite electrodes, 80% active material, with titanium and stainless steel current collectors, recorded at 5 mV/s in 0.65 M* K_2SO_4 *solution. Currents are normalized to the total mass of the composite electrodes*

with stainless steel (0.90 V). Additionally, the shapes of the CVs are similar, showing that there is no significant resistance arising from titanium oxides formed during cycling.

4 Development of binder-free nanocomposites based on carbon nanotubes and MnO_2

4.1 Deposition of MnO_2 on carbon paper–carbon nanotube substrates

Among all the oxides studied for supercapacitor applications, ruthenium oxide produces the highest specific capacitance, values of 760 F/g having been reported [24, 25]. The high cost and possible environmental concerns have limited its commercial application [26]. Being inexpensive and environmentally benign, amorphous hydrous manganese oxide is an attractive alternative for ruthenium oxide in electrochemical capacitor applications. If one Mn atom in MnO_2 is assumed to store one electron, then the theoretical specific capacitance of MnO_2 should be 1370 F/g [27]. Practically, these oxides exhibit specific capacitance of only around one-fifth of the maximum. The primary causes of this low specific capacitance arise from the material's intrinsically low electronic conductivity and its dense morphology [28, 29]. Therefore, the challenge with MnO_2 lies in maximizing its electrochemical utilization. Because of their excellent electric conductivity and high specific surface area, carbon nanotubes (CNTs) are now being combined with MnO_2 to form nanocomposites [26, 30–36].

The current approach to preparing these nanocomposites consists of three steps: (i) the dispersion of CNTs at the manganese oxide surface, (ii) the formation of the composite film with an appropriate binder, and (iii) the assembly of the composite film on a current collector. It is well known that the dispersion is rather difficult and the adhesion of nanotubes to the MnO_2 matrix material remains problematic. Indeed, the effective utilization of CNTs in a composite depends strongly on the ability to disperse the CNTs uniformly throughout the host matrix without destroying their integrity or reducing their aspect ratio. Therefore, the formation of a composite film is not always straightforward and usually requires several trial-and-error steps to obtain a good product. Furthermore, experimental conditions must be optimized to obtain a low contact resistance between the metal oxide/CNT composite and the current collector.

This work aimed to overcome these difficulties by proposing a strategy for the preparation of MnO_2/CNT nanocomposites. For the first time, the direct redox deposition of manganese oxide on multiscaled CNTs/microfibre carbon paper (CP) electrode is reported. The resulting material can be used as binderless electrode for electrochemical capacitors.

4.1.1 Materials synthesis

The solution for redox deposition (0.25 M $KMnO_4$ + 0.5 M H_2SO_4) was prepared as described in the literature [37]. The as-prepared CP-CNT and CP sheets (see section 2.2.1) were dipped in a beaker containing the freshly prepared $KMnO_4 + H_2SO_4$ solution for 30 minutes. The samples were then rinsed with distilled water and dried under vacuum at room temperature for 24 h. Two samples were prepared, denoted as CP-MnO_2 and CP-CNT-MnO_2. The CP and CP-CNT electrodes were subsequently used as substrates for the spontaneous formation of MnO_2 from MnO_4^- ions.

4.1.2 Materials Characterization

The SEM images of a CP-MnO_2 electrode show an aggregation of MnO_2 particles on the fibres of the CP (Figure 7a). The density of these aggregates is low, and a higher magnification (Figure 7b) reveals that they have a diameter of around 1 μm. Because it is well known that the pseudocapacitive reaction of MnO_2 is a surface process [27], small, thin aggregates of MnO_2 will lead to optimal performance.

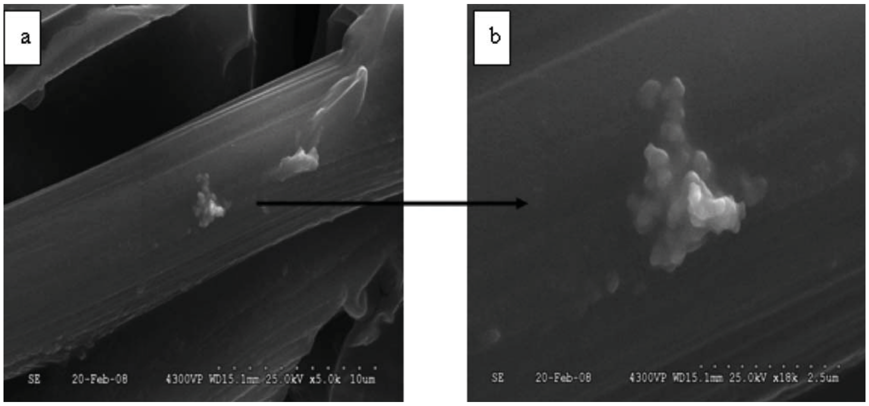

Figure 7: *SEM images of the CP-MnO_2 composite at (a) 5000× and (b) 10,000×.*

The morphology of deposited manganese oxide on the multiscaled CNTs/microfibre CP substrate was also analyzed by SEM. The micrographs and energy dispersive x-ray (EDX) analysis of this electrode system are shown in Figure 8. At low magnification (Figure 8a), the MnO_2 is apparent on the CNT/microfibrous CP substrate, concentrated primarily on the CNT. Higher magnification, Figure 8b, shows that CNTs are well-coated with MnO_2. Figure 8c shows a carbon fibre coated with the CNTs that act as deposition sites for MnO_2 aggregates. Further magnification (Figure 8d) confirms that the CNTs dispersed on carbon microfibres are coated with MnO_2. In Figure 8e, one can see a single CNT partially coated with manganese oxide, and the thickness of MnO_2 deposited layer is approximately 10 nm. The deposition of MnO_2 on CNTs in such thin layers will maximize the material's electrochemical activity. The EDX analysis (Figure 8f) of the CP-CNT-MnO_2 electrode reveals that the atomic ratio of oxygen and manganese in CP-CNT-MnO_2 is 2. Therefore, the as-formed coating is presumably the amorphous hydrous manganese oxide MnO_2. Therefore, the CNTs are the preferred sites for the reduction of MnO_4^- ions.

From the CV (recorded at 1 mV/s), the specific capacitance of the CP-CNT-MnO_2 nanocomposite electrode is 322 F/g, and higher than that of CP-MnO_2, which is 125 F/g. The improved performance of CP-CNT-MnO_2 electrodes is attributed to: (i) the high electrical conductivity of the electrode due to the addition of CNTs, (ii) the deposition of small MnO_2 aggregates on CNTs, maximizing the electrochemical availability of MnO_2, and (iii) the porous structure of nanocomposite, which allows the penetration of the electrolyte deep into the matrix.

Electrochemical impedance spectroscopy (EIS) measurements of the CP-MnO_2 and CP-CNT-MnO_2 electrodes were performed at 0 V *vs*. $Hg/HgSO_4$, producing the Nyquist plots in Figure 9. The Nyquist plots consist of distinct regions: (i) a semicircle in the high to medium frequency region, only for the electrode without the CNT, (ii) a straight line with a slope of 45°, corresponding to the semi-infinite Warburg impedance, which relates ion penetration through the thickness of the porous structure of the electrode [38–40], and (iii) a vertical line at very low frequencies, due to the accumulation of ions at the bottom of the

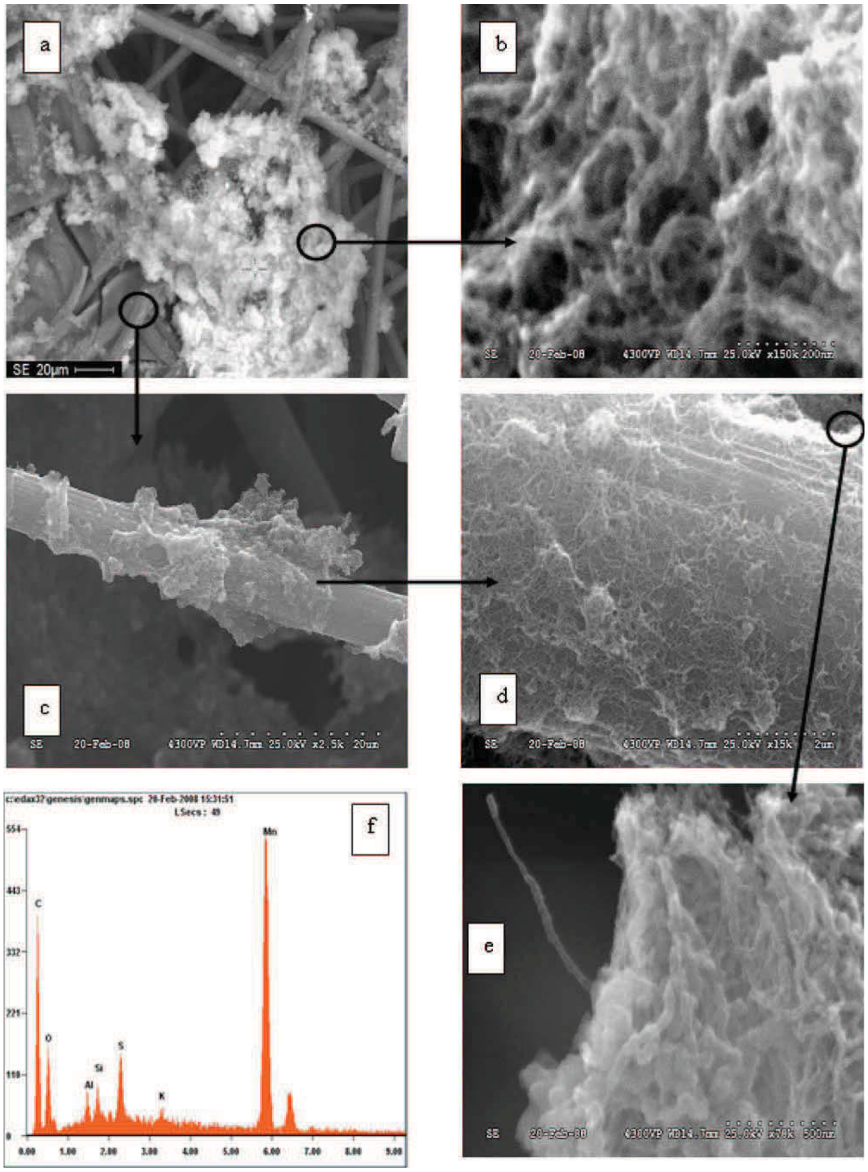

Figure 8: *SEM images and EDX analysis of the CP-CNT-MnO_2 composite.*

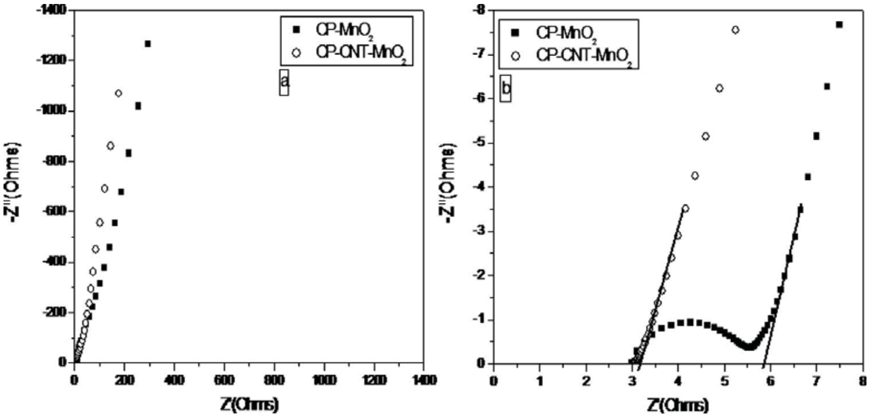

Figure 9: *Electrochemical impedance spectra of CP-MnO_2 and CP-CNT-MnO_2 electrodes in 0.65 M K_2SO_4. Applied voltage: 0 V vs. Hg/$HgSO_4$, frequency range: 100 kHz to 10 mHz. (a) Overall plot, (b) low-frequency zoom.*

pores of the electrode. The almost-vertical line illustrates good capacitive behaviour in the absence of diffusion limitation. The semicircle reflects the sum of the electrolyte resistance and the contact resistance between the active material and the current collector. Simply, this means that a better electrical contact is being made to the current collector in the CP-CNT-MnO_2 electrode; no semicircle is seen for the CP-CNT-MnO_2 electrode. The deposition of a thin MnO_2 layer on CNT allows a better electrical contact compared to an electrode made by the deposition of big MnO_2 aggregates on CP. The factors that determine contact properties between MnO_2 and CNT, and MnO_2 and CP are: (i) the adhesion of MnO_2 to the current collector; the deposited thin film of MnO_2 on CNT has a better adhesion than the big MnO_2 aggregates on CP, and (ii) the high surface contact between MnO_2 and the current collector; a large surface contact surface will result in small contact resistance. In the case of CP-CNT-MnO_2, most of the current flows from MnO_2 to CNT. However, for CP-MnO_2, the current must flow through the bulk of the large MnO_2 particles.

To summarize, low-cost nanocomposite materials based on a simple *in situ* coating technique of a multiscaled CNT/microfibrous CP substrate by manganese oxide were demonstrated. The multiscaled CNT/microfibrous CP substrate efficiently reduced MnO_4 to MnO_2. The specific capacitance of the CP-CNT-MnO_2 nanocomposite electrode was 322 F/g, far beyond that of CP-MnO_2, which was 125 F/g. EIS showed that the addition of CNT improved electrical conductivity and the electrical contact between the active material and the current collector.

4.2 Deposition of nanostructured MnO_2 on carbon nanotubes

Currently, there are effectively two ways to obtain high specific capacitance from manganese oxide. The first is to form nanostructured manganese oxide that yields a specific capacitance in the range of 700 F/g [41–44]. The second is to incorporate carbon nanotubes in the MnO_2 matrix, producing specific capacitances in the range of 325 to 580 F/g [36, 45–47].

This section describes a new low-cost class of binderless nanocomposite materials based on nanostructured metal oxide (manganese oxide) and carbon nanotubes. This nanocomposite is prepared via the electrophoretic deposition (EPD) of CNTs on a stainless steel substrate (see section 2.2.2) followed by direct spontaneous reduction of MnO_4^- ions on the multi scaled SS-CNT substrate to form MnO_2. A key feature of this particular nanocomposite is that it does not require the use of a binder. Commonly, electrodes are fabricated by mixing the active material with a conductivity enhancer and a binder to promote the adhesion of the particles. However, the use of binder and/or other adhesives may occlude some fraction of the surface of the active materials and/or electrically isolate some particles. This CNT-MnO_2 nanocomposite was fabricated directly on the SS substrate without any binder or conductive additives.

4.2.1 Materials synthesis

The solution for redox deposition was 0.25 M $KMnO_4$ in 0.5 M H_2SO_4 and was prepared according to the literature [48]. The SS and SS-CNT sheets were dipped in a beaker containing the freshly prepared $KMnO_4 + H_2SO_4$ solution for either 1 or 30 minutes at 50°C. The resulting deposition samples were rinsed with distilled water and dried *in vacuo* at room temperature for 24 hours. The resulting samples are denoted SS, SS-MnO_2-1, SS-MnO_2-30, SS-CNT-MnO_2-1 and SS-CNT-MnO_2-30.

4.2.2 Materials Characterization

SEM images of the various electrodes are shown in Figure 10. The stainless steel substrate presents a smooth surface (Figures 10a and b), while a rougher morphology is obtained following the electrophoretic deposition of CNTs on its surface (Figures 10c and d). The CNT film is highly porous with open space between the entangled nanotubes although the film appears to coat the entire SS substrate. Both the SS and SS-CNT electrodes were subsequently used as substrate (and reducing agent) for the spontaneous formation of MnO_2 from MnO_4^- ions. The SEM images of the SS-MnO_2-1 electrode shown in Figures 10e and 10f illustrate the deposition of MnO_2 nanowires on the SS substrate.

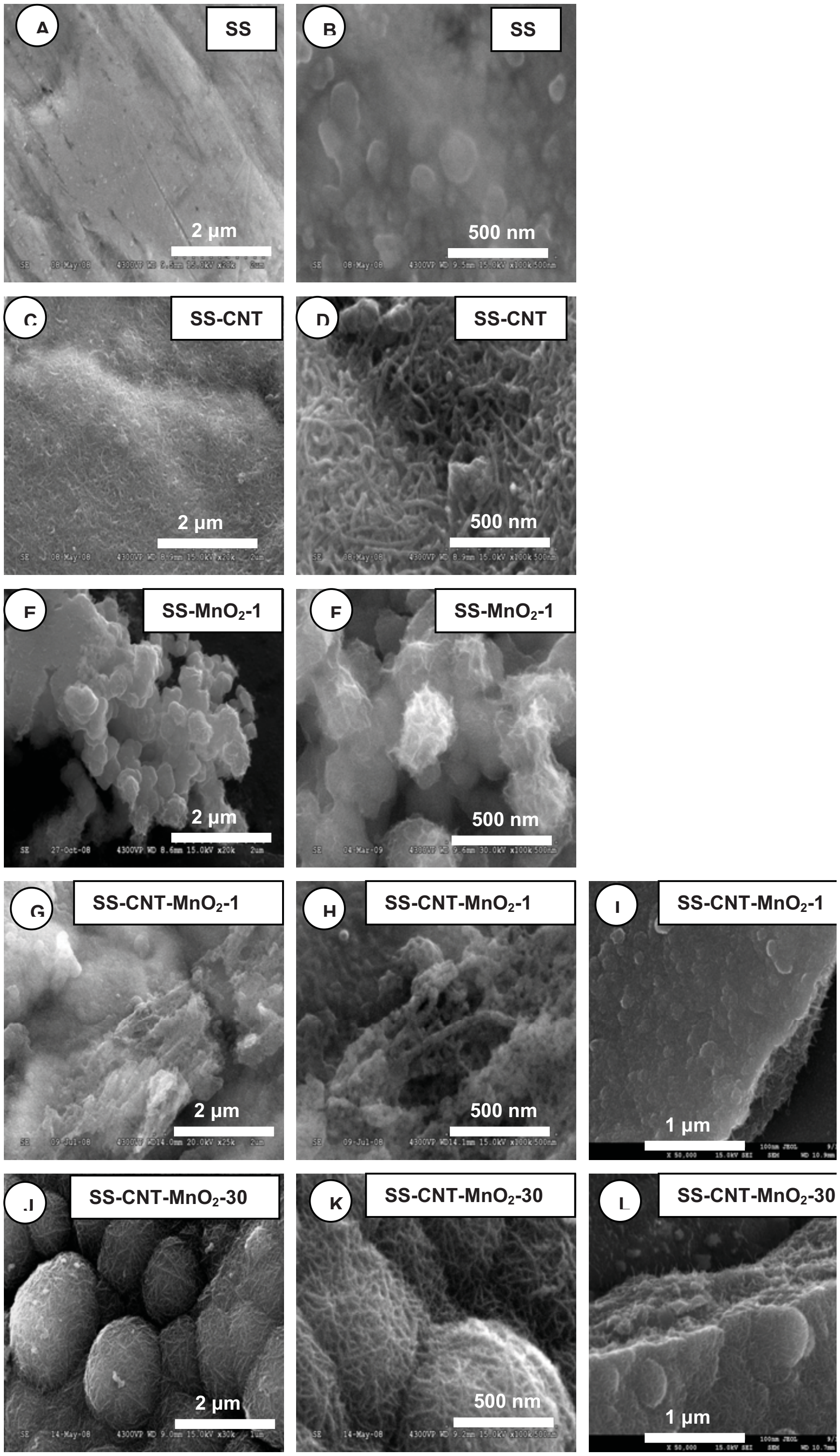

Figure 10: *SEM images of (a,b) SS, (c,d) SS-CNT, (e,f) SS-MnO$_2$-1, (g,h,i) SS-CNT-MnO$_2$-1, and (j,k,l) SS-CNT-MnO$_2$-2*

The SEM images of the SS-CNT-MnO_2-1 sample displayed on Figures 10g, 10h, and 10i show that the carbon nanotubes are covered by manganese oxide layer estimated to be a few nm thick. Presumably, this thin porous layer allows penetration of the electrolyte and maximal accessibility of active material, both of which are very important for electrochemical capacitor applications.

The longer deposition period (30 min) lead to an increased deposition of MnO_2. Figures 10j, k, and l show the SEM images of the SS-CNT-MnO_2-30 electrode. This material is characterized by a nanostructured morphology which consists of manganese oxide nanowires (around 5 nm diameter and longer than 100 nm). In this sample, nanostructured manganese oxide completely covers the carbon nanotubes. Figures 10i and l, indicate that the thickness of the active material (CNT-MnO_2) in the SS-CNT-MnO_2-1 and SS-CNT-MnO_2-30 electrodes is around 300 nm.

Figure 11 (inset) shows the CV of the SS-CNT electrode in 0.65 M K_2SO_4. It exhibits non-ideal capacitive behaviour by its non-rectangular shape. The increase in the current at the positive and negative (for the SS-CNT electrode) potential limits were due to unidentified redox processes. The CV response of the SS-CNT electrode was 5 times larger than that of the bare SS electrode of an equivalent geometric area. Figure 11 shows the CVs for SS-CNT, SS-MnO_2-1, SS-MnO_2-30, SS-CNT-MnO_2-1 and SS-CNT-MnO_2-30 electrodes under the same experimental conditions. The five CVs display an almost rectangular shape over 800 mV even though strong polarization is evident. The SS-CNT electrode shows a specific capacitance of about 145 F/g, which is consistent with values reported for CNT in the literature [49,50]. The specific capacitances of the SS-MnO_2 electrodes are much lower (260–360 F/g) than the SS-CNT-MnO_2 (480–813 F/g).

Figure 12a shows the effect of the scan rate on the CV response of a SS-CNT-MnO_2-30 electrode. The current increases with scan rate, with no significant modification of shape of the CVs at high scan rate. The specific capacitance of SS-CNT-MnO_2 electrodes decreased upon increasing the scan rate (inset Figure 12a). The specific capacitance decreased to 448 F/g at scan rate of 50 mV/s, which is only 55% of that measured at 1 mV/s. This decrease can be attributed to the low conductivity of the MnO_2 layer. The specific capacitance of the SS-CNT-MnO_2-30 electrode decreased to 195 F/g at a scan rate 200 mV/s (results not shown), which is 24% of the value measured at 1 mV/s (813 F/g). Therefore, this nanocomposite electrode shows a rate capability similar to that based on manganese oxide and carbon nanotubes developed in an earlier study [45].

The typical constant current charge–discharge curves presented in Figure 12b shows an initial potential drop that is followed by a linear variation of potential. Specific capacitances determined as a function of the applied current are reported as inset in Figure 12b. The specific capacitance calculated from a constant current of 2.5 A/g was estimated to 869 F/g, which is close to that one calculated from the CV at 1 mV/s. As expected, it can be seen that the capacitance slightly decreased as the charge/discharge current increased.

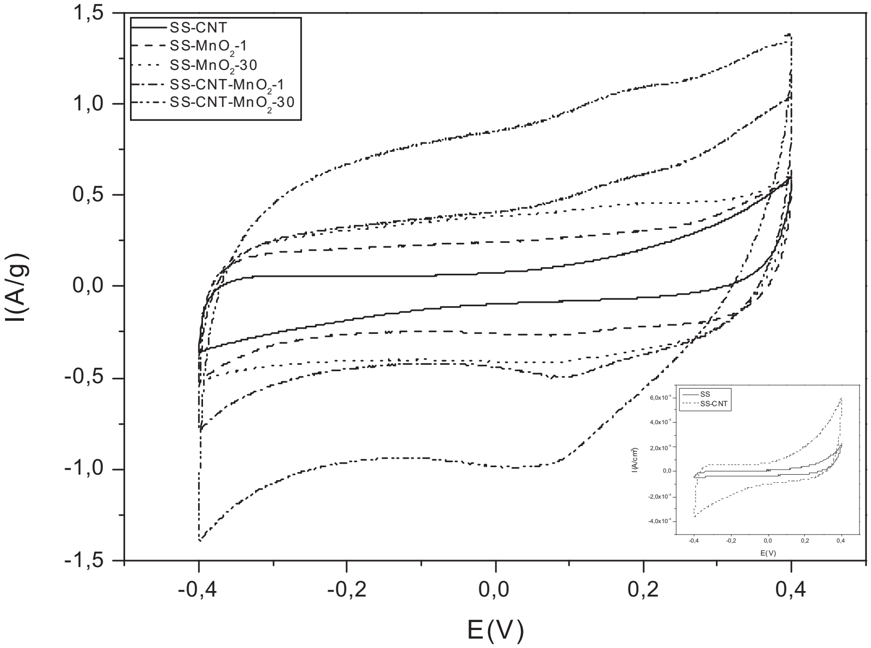

Figure 11: *Cyclic voltamograms of SS-CNT, SS-*MnO_2*-1, SS-*MnO_2*-30, SS-CNT-*MnO_2*-1 and SS-CNT-*MnO_2*-30 electrodes in 0.65 M* K_2SO_4 *aqueous solution at a scan rate of 1 mV/s. Inset: Cyclic voltamograms of SS and SS-CNT electrodes in 0.65 M* K_2SO_4 *aqueous solution at a scan rate of 1 mV/s.*

The capacitance of this nanocomposite is higher than the previously reported value (325 F/g for a nanocomposite electrode based on carbon nanotubes and manganese oxide deposited on carbon paper, CP-CNT-MnO_2 [45]) and is due to: (i) the morphology and mass loading of nanosized manganese oxide, (ii) the use of carbon nanotubes with manganese oxide, (iii) the binderless character of the electrode and the preparation method of the nanocomposite CNT-MnO_2 electrode. First, unlike a dense film, nanosized manganese oxide nanowires provide high specific capacitance due to a porous structure that allows the electrolyte to penetrate deeply into the active electrode material [41–44, 51]. This maximizes the electrochemical utilization of manganese oxide and hence overcomes its principal disadvantage. Second, the mass loading of the SS-CNT-MnO_2-30 and SS-CNT-MnO_2-1 electrodes were lower than that of the CP-CNT-MnO_2 electrode, maximizing the relative electrochemical utilization of manganese oxide. Several studies have demonstrated the beneficial effect of the nanostructured manganese oxide for which specific capacitance fell between 480 and 700 F/g [41–44, 51]. Thus, this nanocomposite electrode shows a 24% improvement in its capacitance compared to those in the aforementioned studies. Third, carbon nanotubes have been recognized as promising materials for electrochemical capacitors due to their interesting properties such as high electric conductivity, good chemical stability and nanosized effect [49, 50]. The use of carbon nanotubes with manganese oxide led to a high specific capacitance because the carbon nanotubes assembly acts as a highly conductive current collector, the continuous porosity serves as a pathway for electrolyte transport, and

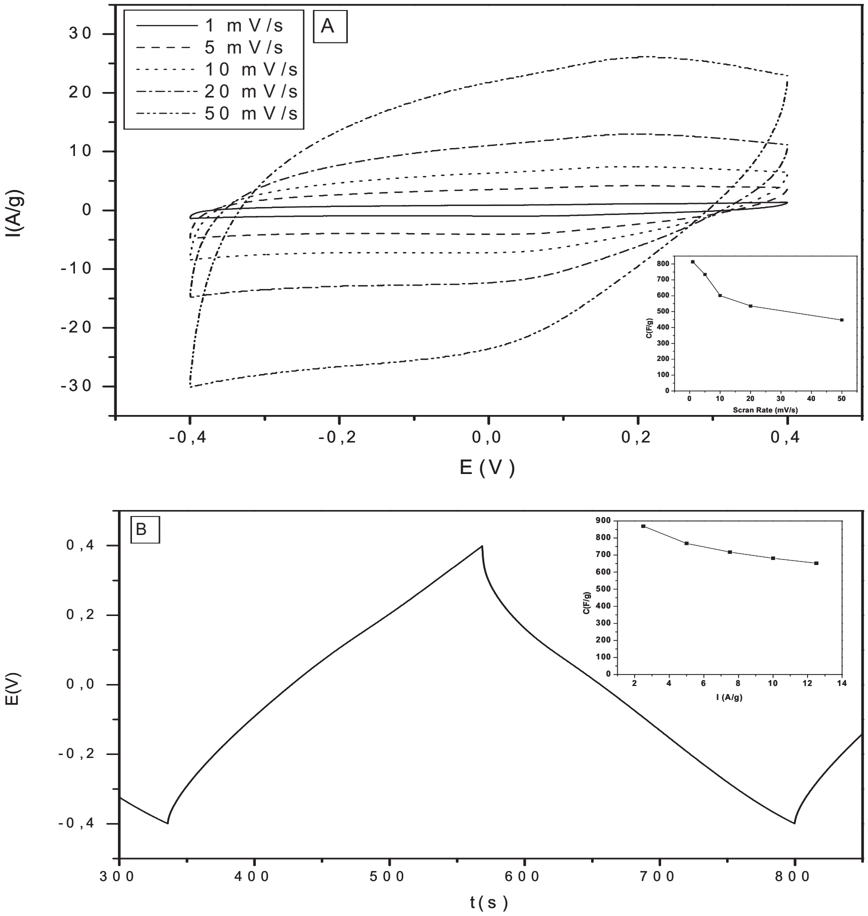

Figure 12: *(a) Cyclic voltammograms of SS-CNT-MnO$_2$-30 electrodes in a 0.65 M K$_2$SO$_4$ aqueous solution at different scan rates. Inset: Variation of the specific capacitance of SS-CNT-MnO$_2$-30 electrode as function of scan rate. (b) Charge–discharge curve (cell voltage versus time) of SS-CNT-MnO$_2$-30 electrode at a current of 2.5 A/g. Inset: Variation of the specific capacitance of SS-CNT-MnO$_2$-30 electrode as a function of applied current.*

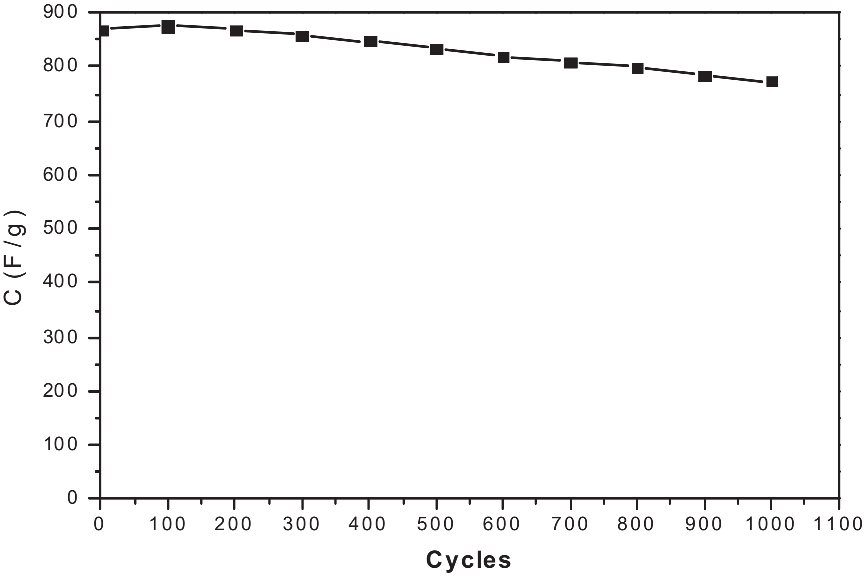

Figure 13: *Variation of the specific capacitance of a SS-CNT-MnO_2-30 nanocomposite electrode as function of cycle number. Electrolyte: 0.65 M K_2SO_4 aqueous solution, charge and discharge at a current of 2.5 A/g.*

the nanostructured MnO_2 minimizes the transport distance for ions into the oxide [52]. Several studies have reported the beneficial effect of the combination of manganese oxide with carbon nanotubes, for example, the specific capacitance of the MnO_2 in a MnO_2-CNT nanocomposite was as high as 580 F/g [36]. Finally, the binderless character of the electrode and the preparation method of the CNT-MnO_2 nanocomposite allowed the increase of the specific capacitance. Conventional methods of preparation of these nanocomposites comprise three steps: (i) dispersion of CNTs at the manganese oxide surface, (ii) formation of composite films with an appropriate binder, and (iii) assembly of the composite films on a current collector. It is well known that the dispersion is rather difficult and the adhesion of nanotubes to the MnO_2 matrix material still present considerable challenges. Indeed the effective utilization of CNTs when used in a composite depends strongly on the ability to disperse the CNTs individually and uniformly throughout the host matrix without destroying their integrity or reducing their aspect ratio. In the present work, the nanosized manganese oxide was directly deposited on CNTs which were previously deposited on the current collector to allow a better distribution of the nanosized manganese oxide on the surface of CNTs and also avoid the use of a binder. The combination of the three previous factors leads to a 24% increase of the specific capacitance of manganese oxide but which is still far from the theoretical specific capacitance of MnO_2, around 1370 F/g [27].

The cycling stability of the SS-CNT-MnO_2-30 nanocomposite electrode was also investigated for 1000 galvanostatic charge-discharge cycles in 0.65 M K_2SO_4 electrolyte (Figure 13). A slight decrease of the specific capacitance is observed. Thus, this nanocomposite electrode shows a relatively good cycling stability.

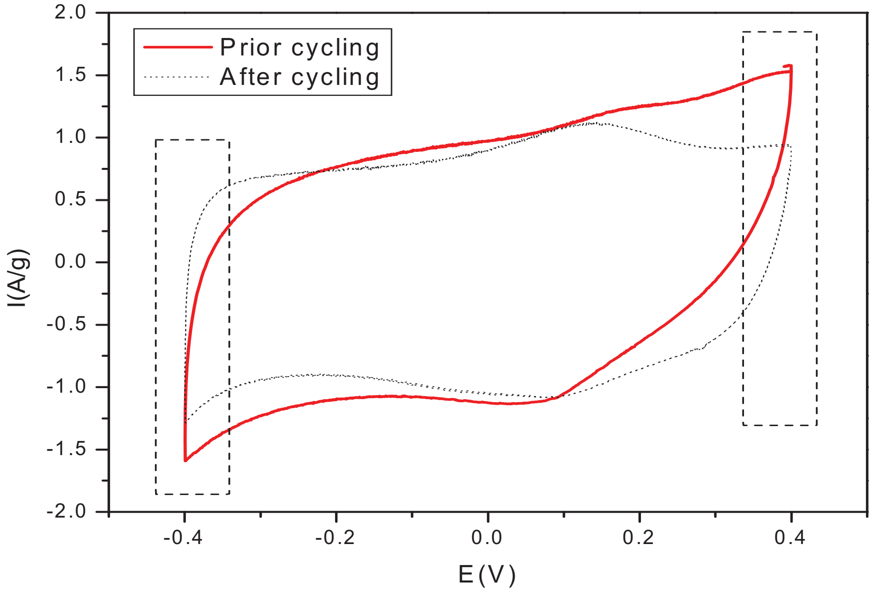

Figure 14: *Cyclic voltammograms recorded prior and subsequent to cycling experiments shown in Figure 12 for a SS-CNT-MnO_2 electrode in 0.65 M K_2SO_4 at a potential scan rate of 1 mV/s.*

Figure 14 presents cyclic voltammograms recorded prior and subsequent to cycling experiments for a SS-CNT-MnO_2-30 electrode in 0.65 M K_2SO_4 at a potential scan rate of 1 mV/s. It is evident that they are minor changes between the CVs with only a 10% loss of capacitance, suggesting a good high electrochemical stability for this nanocomposite electrode. The loss of capacitance is in agreement with the one calculated from galvanostatic charge-discharge. The dotted boxes drawn in Figure 14 presents the potential regions where deviations from an ideal behaviour can be noticed. For the sample before cycling, the deviation is higher and become less apparent after cycling. This can be attributed to the improvement of the electric conductivity upon cycling due to repetitive insertion and deinsertion of ions.

SEM images of the SS-CNT-MnO_2-30 electrode following cycling are shown in Figure 15. Two different morphologies were observed and the first one is presented in Figure 15b with further magnification in Figure 15c. This morphology is similar to one seen prior to cycling (Figure 10e), indicating that cycling does not change the morphology of the material of this region. For the second region, Figures 15d,e, and f demonstrate a clear alteration of the morphology upon cycling (Figure 10e). After cycling, the morphology shows a nanostructure in a three-dimensional network (Figure 15d). Further magnification in Figure 15e,f shows a three-dimensional network composed of cross linked nanoneedles or nanowires, the pores between the nanoneedles are found to be approximately 100 to 200 nm in diameter. More encouragingly, such manganese dioxide nanostructures are thought to be beneficial to ionic charge transport within the coating.

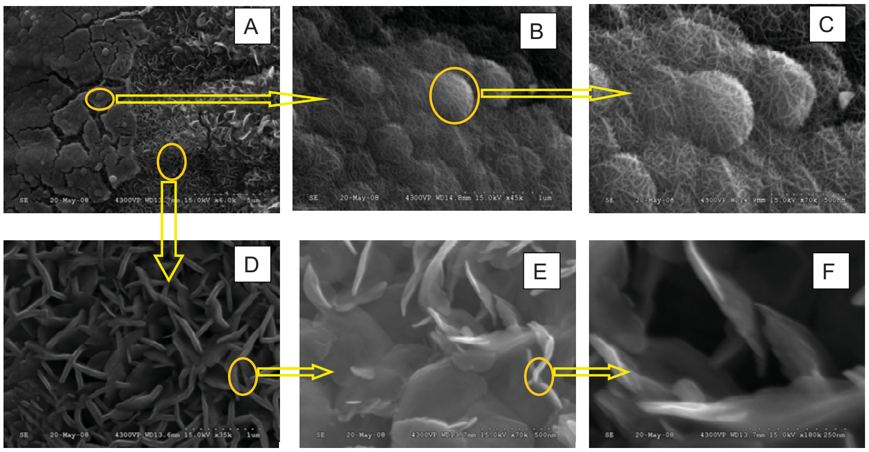

Figure 15: *SEM images of the cycled SS-CNT-MnO_2-30 electrode.*

5 Thin film mixed oxide electrodes

The objective of this section is the development of alternative material for RuO_2, which is limited by a high cost that prevents its widespread use as active electrode material in electrochemical capacitors. To reach this objective, we prepared mixed oxide based on ruthenium and manganese oxide, $Ru_xMn_{1-x}O_2$ thin films for which the parameter x was varied progressively from 1 to 0 in order to decrease the content of the costly ruthenium metal. These materials should have good electrochemical characteristics such as high specific capacitance and a large voltage window in the range of at least 1.4 V. It is relevant to note that thin films were investigated, instead of thicker composite film electrodes, for potential applications in high power electrochemical capacitors.

5.1 Materials synthesis

Manganese (II) nitrate tetrahydrate ($Mn(NO_3)_2 \cdot 4\,H_2O$; Aldrich) and ruthenium (III) nitrosylnitrate, ($Ru(NO)(NO_3)_3$; Alfa Aesar, Ru, 31.3% min) were used as precursors for the preparation of the mixed oxides. Titanium plate (Good Fellow; > 99.6%, thickness 0.05 mm) was used as the substrate. The precursor solutions were obtained from a mixture of $Mn(NO_3)_2 \cdot 4\,H_2O$ and $Ru(NO)(NO_3)_3$ in 0.1 M HNO_3 (ACS; EMD chemicals) in order to obtain a cationic concentration of 0.16 M and varying a molar fraction of Ru between 0 to 1. The electrolytic solutions were prepared from concentrated H_2SO_4 (Fisher) or from Na_2SO_4 (Anachemia Canada) and Nanopure H_2O (18.2 MΩ·cm, Millipore Corporation). The degreasing solution was composed of concentrated H_2SO_4 and H_2O_2 (30% solution, ACS; Anachemia Canada) in a 2:1 volume ratio. The titanium substrates were subjected to a mechanical polishing with emery paper. Afterward, they were immersed in the degreasing solution for 30 s then rinsed with distilled water and dried at 90°C for 15 min. Each face of the substrate was modified by application of a layer of precursors solution

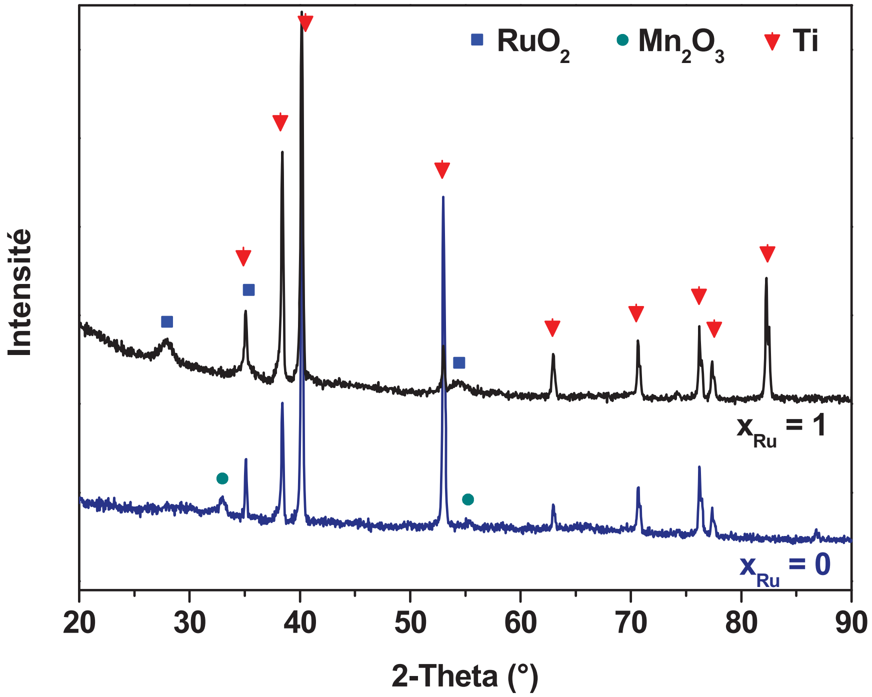

Figure 16: *X-ray diffraction patterns for ruthenium (x_{Ru}=1) and manganese (x_{Ru}=0) oxides on a titanium substrate.*

by using a brush. To ensure complete decomposition of the metallic precursors, a thermal treatment was applied at 150°C for 10 min. A total of 12 layers were deposited in the same way. After the final deposition, a thermal treatment was applied at 450°C for 1 h. Three samples for each solution precursor were prepared, where x_{Ru} = 1, 0.8, 0,6, 0.5, 0.4, 0.2, and 0. The average mass loading for each film was 0.3±0.1 mg/cm2. The relatively large standard deviation is due to the procedure being used for the preparation of the electrodes.

5.2 Materials characterization

Figure 16 shows XRD patterns for the Ti substrate coated with pure ruthenium and manganese oxides thin films. In addition to the peaks associated to the titanium substrate, the XRD pattern for the manganese oxide electrode also shows broad and low intensities peaks at 32.9 and 55.2° that are attributed to the presence of Mn_2O_3, which is formed by thermal decomposition of manganese nitrate at 450°C [53]. The same phase was also produced for oxide films generated by sol-gel method by using manganese acetate as precursor and using a thermal treatment in air at temperature higher that 250°C [54]. Finally, the formation of tetragonal RuO_2 phase on the titanium substrate is confirmed by the presence of diffraction peaks at 27.9, 35.1 and 54.3° [55].

XRD patterns for $Ru_xMn_{1-x}O_2$ thin film coated titanium substrates are presented in Figure 17 for $0.2 < x_{Ru} < 0.8$. Interestingly, no peaks that could be attributed to the presence

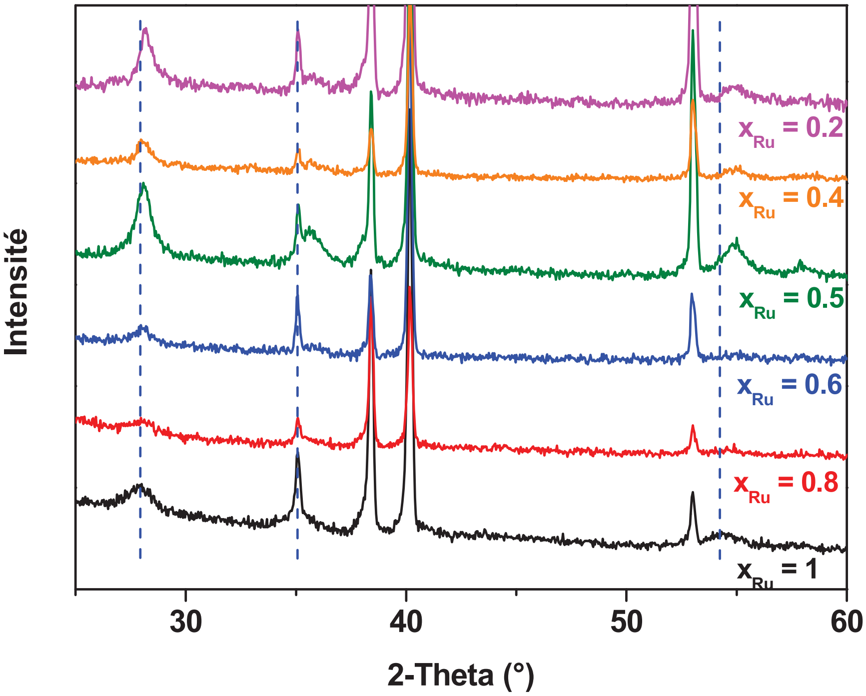

Figure 17: *X-ray diffraction patterns for $Ru_xMn_{1-x}O_2$ thin film coated titanium substrates The ruthenium fraction is indicated (x_{Ru}=0.2, 0.4, 0.6, 0.8, and 1).*

of the Mn_2O_3 phase are detected. However, additional peaks at 28.1, 35.6 and 54.8° are observed. These peaks are found at slightly higher 2Θ values than those mentioned above for RuO_2 and in fact they are located between those of RuO_2 and $\beta-MnO_2$ which is also characterized by a tetragonal phase [56]. These XRD patterns are in very good agreement with those reported for materials produced by thermal decomposition of ruthenium and manganese nitrate salts at 370°C [57]. The materials possess a rutile structure and the presence of the $\beta-MnO_2$ phase is also noticed when the Ru fraction is smaller than 0.7. In conclusion, the XRD data confirm the presence of a mixed oxide despite the relatively low intensity of the peaks of the XRD patterns.

Electrochemical measurements were carried out in a conventional three-electrode Pyrex glass cell. $Ru_xMn_{1-x}O_2$ films supported on titanium substrates prepared as described in the previous section were used as working electrode, while a gold wire was used as counter electrode and a saturated calomel electrode (SCE) as reference electrode. The electrochemical characterization was carried out in either 0.5 M H_2SO_4 or 0.5 M Na_2SO_4.

Figure 18 shows the cyclic voltammograms of $Ru_xMn_{1-x}O_2$ (x_{Ru}=0.2, 0.4, 0.6, 0.8, and 1) electrodes in 0.5 M H_2SO_4 which exhibit a capacitive behaviour over 1000 mV. The cyclic voltammogram of Ti/RuO_2 electrode has approximately the same shape as those reported for RuO_2 electrodes prepared by a sol gel method at a temperature of 400°C [25]. The specific capacitance of the electrodes determined from the cyclic voltammograms are

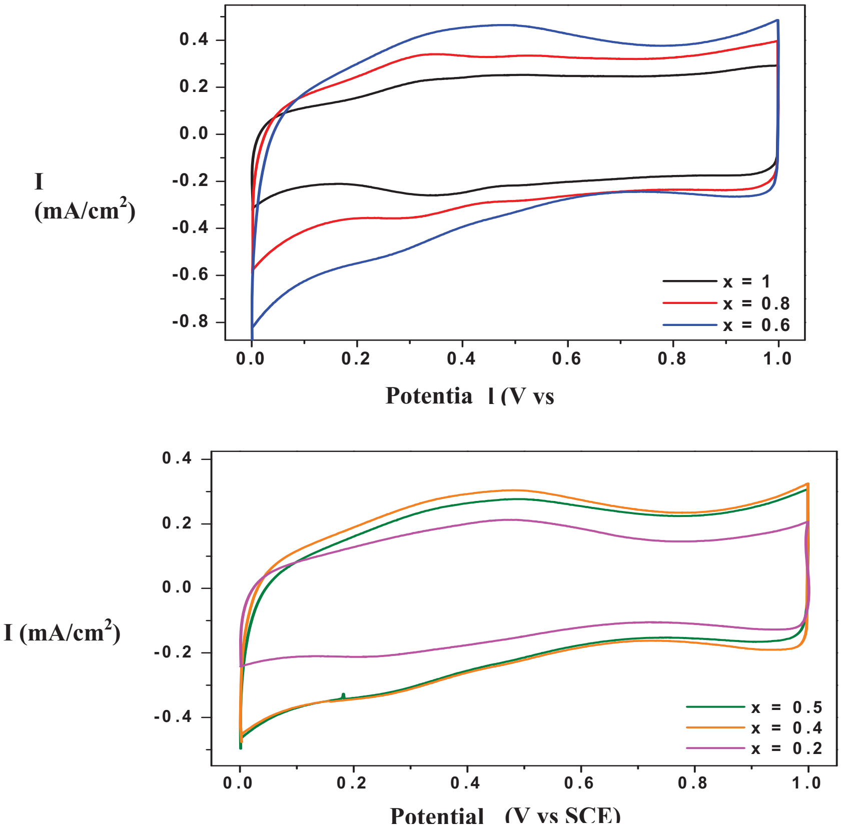

Figure 18: *Cyclic voltammograms of Ti/Ru$_x$Mn$_{1-x}$O$_2$ electrodes recorded between 0 and 1.0 V vs. SCE in 0.5 M H$_2$SO$_4$ at scan rate 10 mV/s. (a) x=1, 0.8, 0.6; (b) x=0.5, 0.4, 0.2.*

Table 4: *Specific capacitance of Ti/*$Ru_xMn_{1-x}O_2$ *electrodes in 0.5 M* H_2SO_4 *and 0.5 M* Na_2SO_4 *electrolytes evaluated from cyclic voltammograms recorded at a scan rate of 10 mV/s.*

Electrode Material $Ru_xMn_{1-x}O_2$	C_{sp} (F/g) 0.5 M H_2SO_4	C_{sp} (F/g) 0.5 M Na_2SO_4
1	40	68
0.8	104	25
0.6	174	19
0.5	97	17
0.4	77	38
0.2	83	44
0	—	42

listed in Table 4. The specific capacitance of Ti/RuO_2 is 40 F/g and is comparable to that reported for crystalline RuO_2 annealed at 400°C [25]. On the other hand, in the latter study it has been shown that a specific capacitance of 720 F/g can be obtained for amorphous ruthenium oxide prepared by a sol gel method at a temperature of 150°C [25]. In contrast to the crystalline materials, the intercalation of protons is possible into the bulk of the amorphous ruthenium oxide and explains the larger capacitance for the "low temperature" RuO_2 [25]. Table 4 shows that the specific capacitances of Ti/$Ru_xMn_{1-x}O_2$ electrodes are higher than that of the Ti/RuO_2 electrode. The $Ru_{0.6}Mn_{0.4}O_2$ electrodes show the highest specific capacitance (174 F/g).

In order to evaluate the full electrochemical domain of $Ru_xMn_{1-x}O_2$ electrodes, cyclic voltammograms were recorded over a larger potential window between the hydrogen and oxygen evolution reactions (Figure 19). For all $Ru_xMn_{1-x}O_2$ electrodes, the onset of the oxygen evolution reaction occurs at around 1.15 V and the evolution of hydrogen at -0.4 V. Therefore, the potential window of $Ru_xMn_{1-x}O_2$ electrodes is independent of the Ru/Mn ratio of the electrode and found to be about 1.5 V. Figure 19 shows that the shape of the cyclic voltammogram changes slightly upon addition of manganese to the mixed oxide. Indeed, the cathodic wave observed at -0.15 V for the Ti/RuO_2 disappeared and the capacitance in the potential range between -0.4 and 0 V decreased when the manganese content of the Ti/$Ru_xMn_{1-x}O_2$ electrodes increased.

Since application of these materials in neutral aqueous electrolytes would be of potential interest for environmentally friendly electrochemical capacitors, the cyclic voltammogram of the Ti/$Ru_xMn_{1-x}O_2$ thin film electrodes was also recorded in aqueous 0.5 M Na_2SO_4 electrolyte. Figure 20 presents the cyclic voltammograms of $Ru_xMn_{1-x}O_2$ electrodes in 0.5 M Na_2SO_4. An almost rectangular shape is recorded for the Ti/RuO_2 electrode over a potential window ranging from -0.2 to 0.9 V, which is smaller than that found in acidic media. The same observation can be made for all the other electrodes. The shape of the

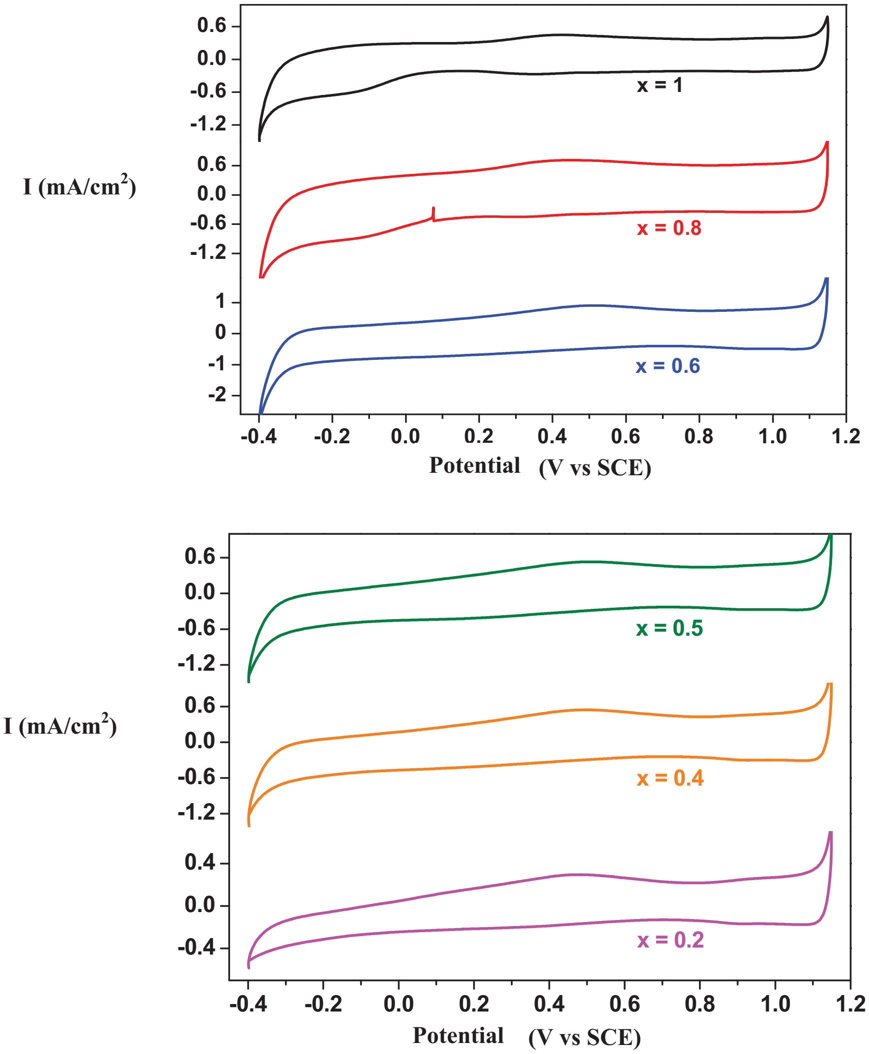

Figure 19: *Cyclic voltammograms of Ti/*$Ru_xMn_{1-x}O_2$ *electrodes recorded between* −0.4 *and 1.15 V vs. SCE in 0.5 M* H_2SO_4 *at scan rate 10 mV/s.*

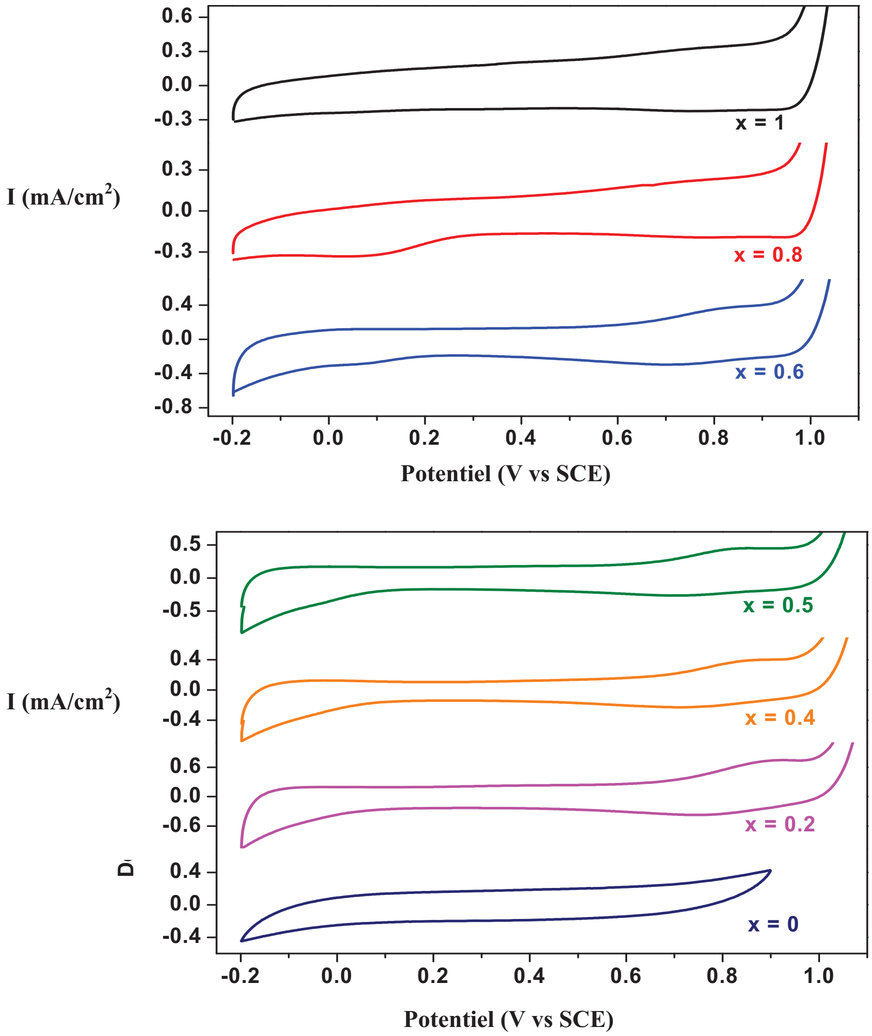

Figure 20: *Cyclic voltammograms of Ti/$Ru_xMn_{1-x}O_2$ electrodes recorded between −0.4 and 1.15 V vs. SCE in 0.5 M Na_2SO_4 at scan rate 10 mV/s.*

cyclic voltammogram changed upon addition of manganese and redox peaks and waves are observed close to the potential limits of the cyclic voltammogram. A more detailed understanding of the redox processes associated to these waves would require more work. Finally, the cyclic voltammogram for the manganese oxide electrode is in agreement with literature data [58]. However, the capacitance value (Table 4) is much smaller than those reported for hydrous manganese dioxide and is consistent with the presence of Mn_2O_3.

In this section, $Ru_xMn_{1-x}O_2$ thin film electrodes have been prepared by thermal decomposition at 450°C of a mixture of ruthenium and manganese salts at the surface of a Ti substrate. XRD patterns have demonstrated the formation of a mixed oxide phase which is distinct from those found for the pure ruthenium and manganese oxide-coated titanium surfaces. It is important to note that the potential windows of these electrodes is 1.5 V in aqueous 0.5 M H_2SO_4 electrolyte and independent of the Ru/Mn ratio of the mixed oxides. The knowledge of the full potential window of an electrode material is crucial for application of the material in asymmetric electrochemical capacitor. Also, the $Ru_{0.6}Mn_{0.4}O_2$ electrode has been shown to have the highest specific capacitance in acidic electrolyte and higher capacitances were found in acidic electrolyte. Further work is needed to optimize the procedure for the preparation of these electrode materials.

6 Effect of MnO_2 loading on electrochemical characteristics

6.1 Materials synthesis

Manganese dioxide has been found to be a promising material as active electrode materials in electrochemical capacitors. Nonetheless, this material has some drawbacks which severely hamper the development of commercial devices. A major issue is related to its relatively poor conductivity and approaches to circumvent this problem are investigated in this section. More specifically, the work focused on the improvement of both the electronic and ionic conductivities of the composite electrodes. To this end, we have investigated the effect of the addition of carbon conductors such as acetylene black, carbon nanotubes and vapor grown carbon fibres as well as Nafion to increase both the electronic and ionic conductivities, respectively. The goal of this study is to determine the effect of the composition of the mixture on the microstructure of the materials used for the fabrication of the composite electrodes and to try to establish a correlation between the pore texture of the materials and the electrochemical performance of the resulting composite electrodes.

6.1.1 Synthesis of MnO_2

The synthesis of amorphous, hydrated manganese dioxide (α-$MnO_2 \cdot xH_2O$) is carried out by mixing a 0.17 M solution of potassium permanganate ($KMnO_4$) and a 0.15 M solution of manganese(II) acetate $Mn(CH_3COO)_2$. The following reaction occurs:

$$\mathrm{Mn(VII)} + 1.5\mathrm{Mn(II)} \longrightarrow 2.5\mathrm{Mn(IV)}$$

The reaction was carried out for 6 h under constant stirring of the solution. The dark brown precipitate was filtered with a ceramic filter, washed several times with deionised water, and then dried at 100°C for 12 h.

6.1.2 Composite electrode preparation

In this work, the active material (MnO_2), the conductor additive (carbon) and the binder polymer were mixed together in presence of ethanol. We have tested acetylene black (Alfa

Aesar, 80 m^2/g), carbon nanotubes (Aldrich, MWCNT) and carbon nanofibres (Showa Denko, Vapor Grown Carbon Fiber (VGCF), 13 m^2/g) as conductor additive. The polytetrafluoroethylene (PTFE) in solid form (Aldrich) and in solution (aqueous solution 60%) as well as Nafion 117 (Fluka, 5%) were used as binder. Two ratios were tested: 60% MnO2 / 30 carbon / 10% binder, and 75% MnO_2 / 15% carbon / 15% binder. In the case of the samples with Nafion, it was not possible to form a paste such as the one required for the fabrication of composite electrodes, and consequently a mixture of Nafion and PTFE (3:1) was used as binder. The composite paste was rolled and cut in 1 cm^2 pieces. Films cut out of the sheet were cold-pressed at 10 ton/cm^2 for 1–2 min onto a stainless steel 340 (Alfa Aesar) current collector.

6.2 Materials characterisation

6.2.1 Pore texture

Nitrogen gas adsorption measurements at 77 K were used for the determination of the surface area and pore size distribution of various porous materials; the compounds alone (manganese oxide and carbons) and the different mixtures of these compounds.

6.2.2 Manganese oxide

The nitrogen gas adsorption isotherm of manganese oxide is shown in Figure 21. According to the IUPAC classification, this is a type IV isotherm, which is typical of mesoporous solids. The histogram of the pore size distribution shown in Figure 22 confirms the mesoporous character of the synthesized manganese oxide powder.

6.2.3 Carbons

The nitrogen gas adsorption isotherm of each carbons (*e.g.*, acetylene black, carbon nanotubes and vapor grown carbon fibres) are presented in Figure 23. According to the IUPAC classification, these are type II isotherms and characteristic of non porous adsorbents solids. Figure 24 presents the histogram of the pore size distribution for each carbons. For acetylene black, one can observe that most of the pores are in the range 20 to 40 Å with an additional contribution in the micropores (smaller than 20 Å) and larger mesopores (larger than 60 Å) range. For the carbon nanotubes, the distribution is mostly found in the mesopore range. Finally, the carbon nanofibres are characterized by a broader distribution of their pores. Thus, since these carbonaceous materials are characterized by various pore textures, it will be interesting to determine the role that they may play on the electrochemical performance of composite electrodes.

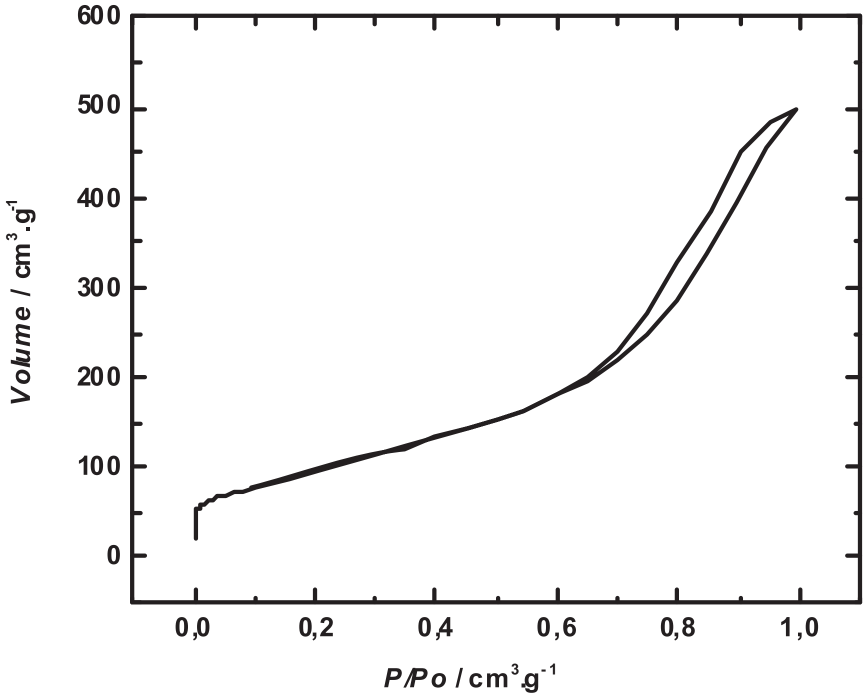

Figure 21: *Nitrogen adsorption isotherm of the manganese oxide powder.*

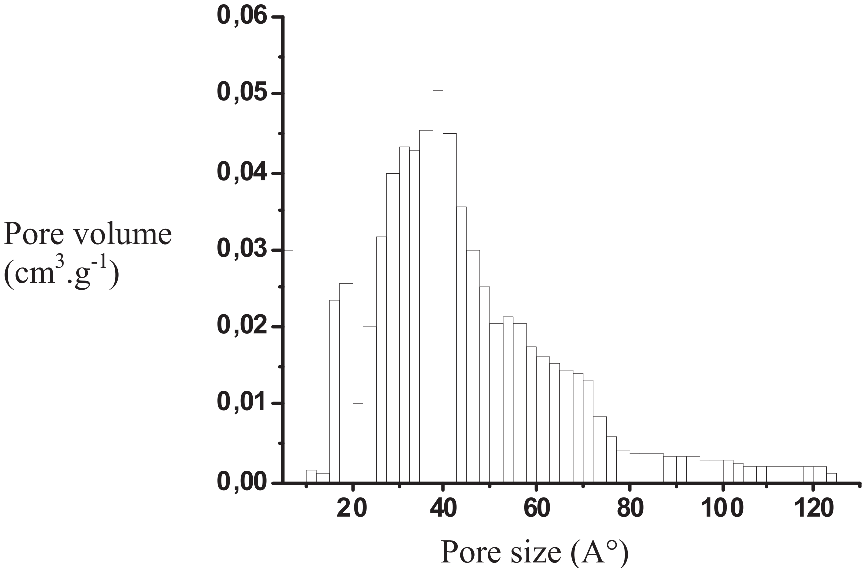

Figure 22: *Pore size distribution of manganese oxide.*

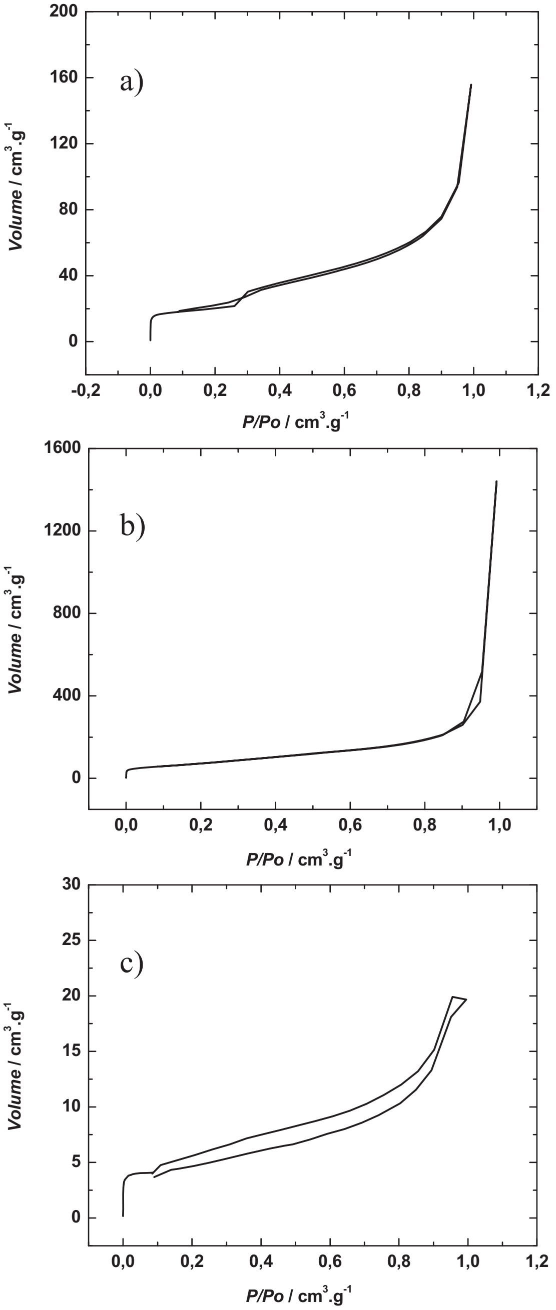

Figure 23: *Isotherm adsorption of various carbon samples: (a) acetylene black, (b) carbon nanotubes, (c) carbon nanofibres.*

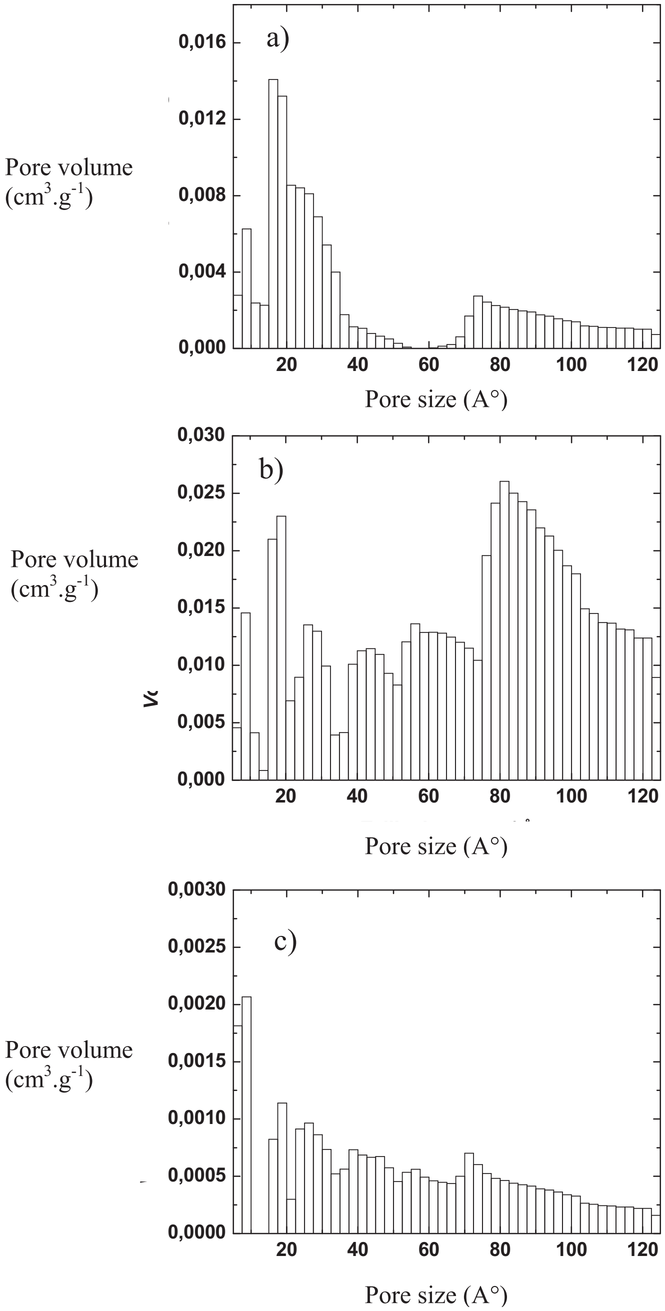

Figure 24: *Pore size distribution of various carbon samples: (a) acetylene black, (b) carbon nanotubes, (c) carbon nanofibres*

6.2.4 Mixture composites

Mixtures of 60% w/w MnO_2, 30% w/w of the conductor additive and 10% w/w of the binder were prepared and the adsorption isotherm of these mixtures are presented in Figure 25. The curves of mixture are characterized by the presence of micropores ($P/P_0 < 0.5$). Between 0.05 and 0.6 cm^3/g, a gradual increase of adsorbed volume of nitrogen is observed. For the mixture prepared with carbon nanotubes, this region corresponds to the nitrogen adsorption on the external surface of the composite, filling the space between the nanotubes and the mesoporous domains of the open nanotubes and MnO_2. For samples with Nafion, the hysteresis is less clearly less pronounced and even absent for carbon nanofibres. This is an indication that the mesopores are strongly affected by the addition of this binder polymer. For samples prepared by using PTFE as binder, the adsorption desorption branches of the isotherms diverge to form an hysteresis for P/P_0 larger than 0.6. This is due to the capillary condensation in the mesopores.

Pore size distribution diagram is an efficient tool to determine the nature of pores in each composite. Figure 26 shows a series of histograms for various mixtures together with the histograms of the individual materials. Qualitatively, the profile of the pore size distribution of the mixture is in agreement with the profile distribution of the individual components (*e.g.*, manganese oxide and carbon) and their ratio in the mixtures. Moreover, as seen directly on the isotherms, it seems that Nafion affects more importantly the pore size distribution than PTFE, especially in the region of small pores.

Plots of the cumulated specific surface areas presented in Figure 27 are also very instructive and demonstrate that most of the surface area can be attributed to pores smaller than 10 nm.

Table 5 shows the BET specific surface area of manganese oxide, carbon nanotubes, acetylene black, vapor grown carbon fibres and the mixtures. The specific surface area of manganese oxide is 320 m^2/g. The carbons used in this work have a specific surface area of 280, 86, and 21 m^2/g for CNT, AB and VGCF, respectively. Table 5 also shows that the surface area of the mixtures is always lower than the value found for MnO_2, indicating that the addition of the carbon conductor does not open its porosity and promote access to a larger surface of the oxide. Furthermore, the addition of Nafion as binder adversely affected the BET surface area of the mixtures. The surface area of the mixtures were also estimated from the values of the individual components and their proportion in the mixtures by assuming a linear combination of the BET surface areas and that the binder does not contribute to the total surface area. Table 5 also reports these calculated BET surface areas which are found to be systematically larger than the measured values. The decrease of the surface areas relative to the expected values can be attributed to the binder which blocks the access to the pores and the surface of the materials to the nitrogen gas molecules, with a more significant effect by Nafion relative to PTFE. In addition, it can be seen that the decrease depends also on the nature of the carbon materials and follows the order: AB<CNT<VGCF.

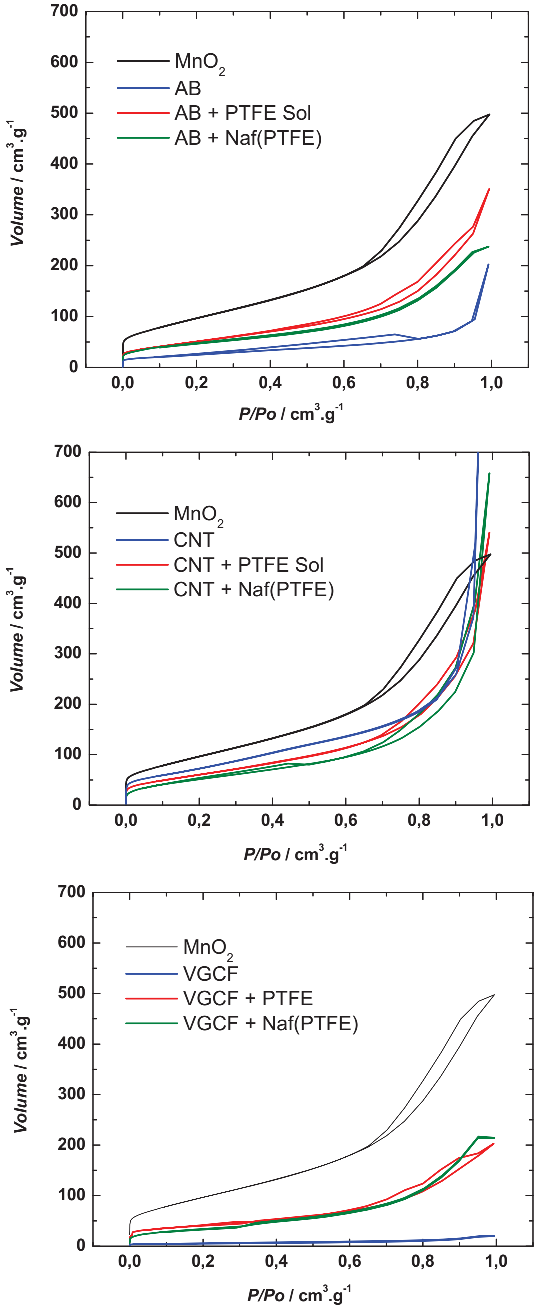

Figure 25: *Adsorption isotherms of different mixtures and each individual components.*

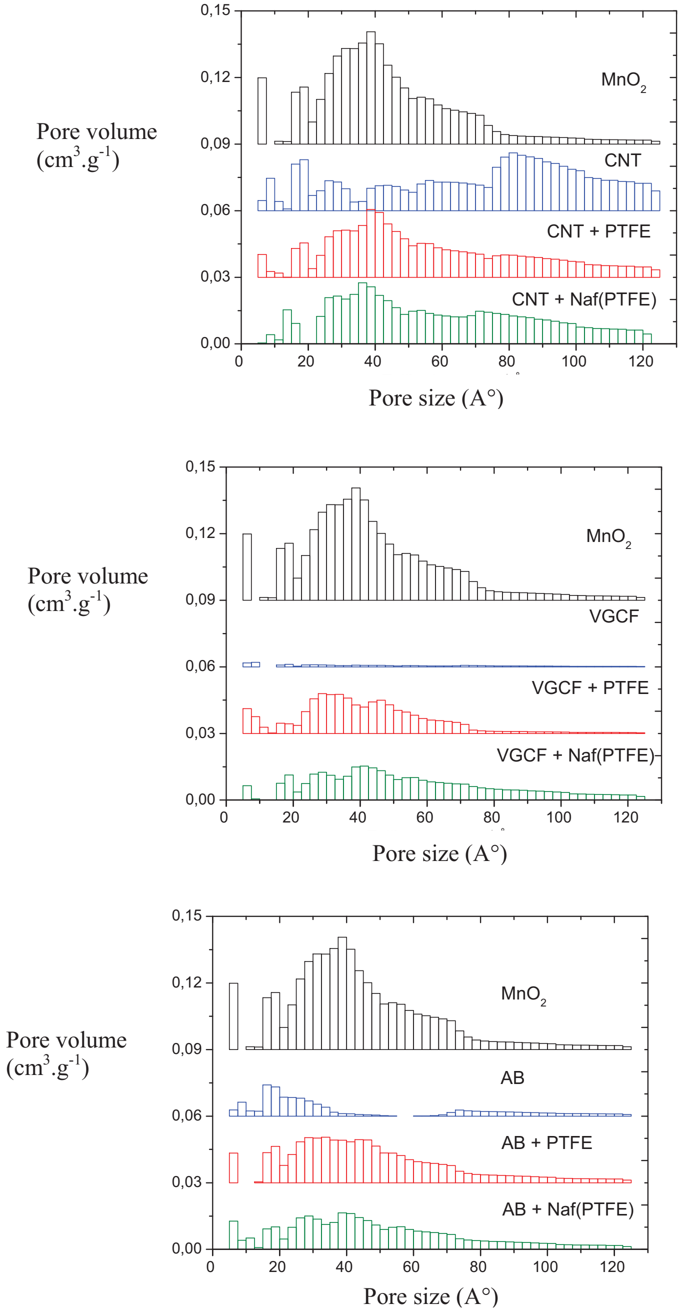

Figure 26: *Pore size distribution of various mixtures and each individual components.*

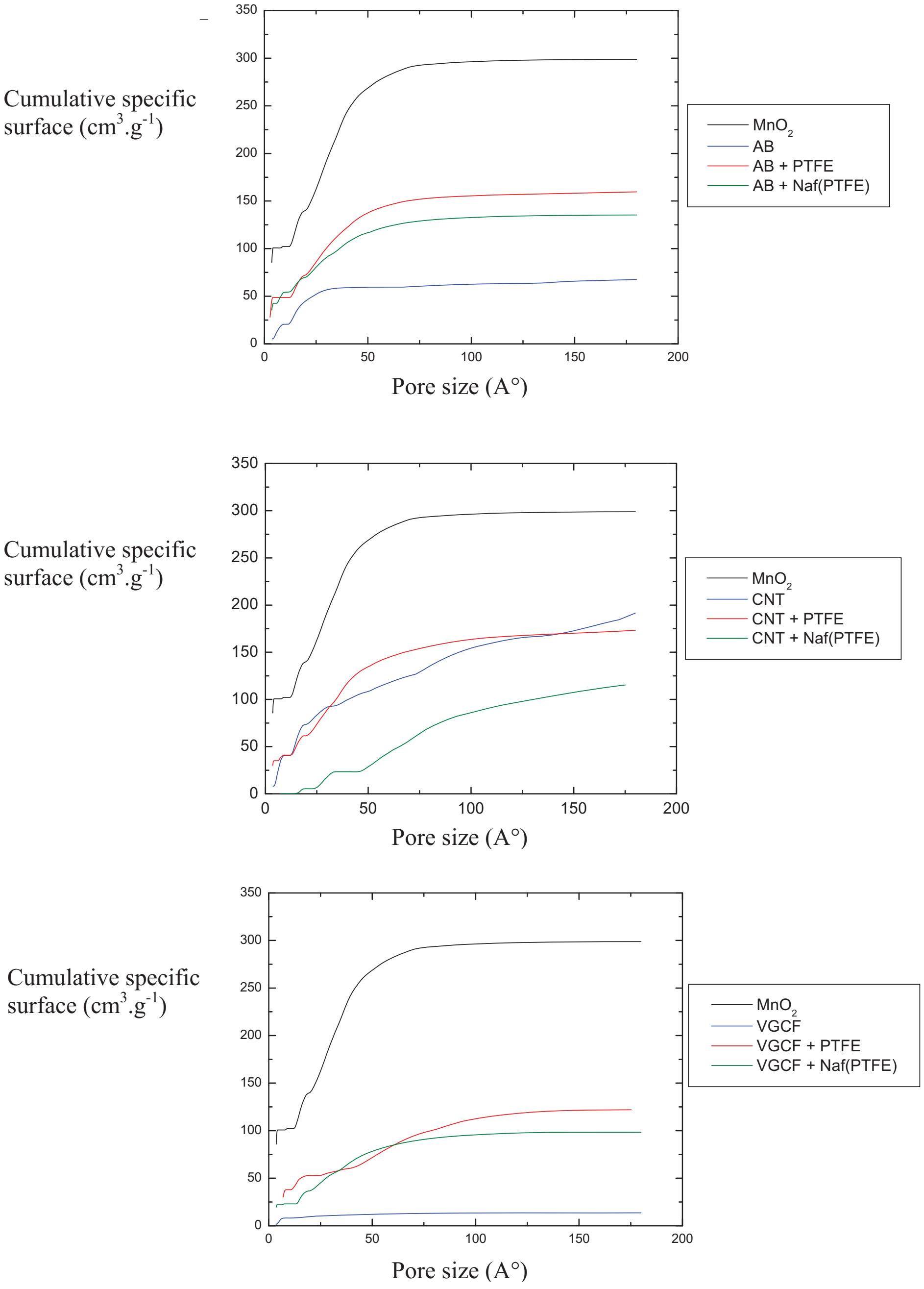

Figure 27: *Cumulated surface area as a function of the pore size for various single materials and mixtures.*

Table 5: *Pore texture for various samples.*

Sample	Measured S_{BET} (m^2/g)	Calc'd S_{BET} (m^2/g)	Δ (m^2/g)
MnO_2	320		
CNT	280		
AB	86		
VGCF	21		
MnO_2–AB–PTFE(s)	190	218	-28
MnO_2–AB–Naf:PTFE	175	218	-43
MnO_2–CNT–PTFE(s)	230	276	-46
MnO_2–CNT–Naf:PTFE	196	276	-80
MnO_2–VGCF–PTFE(s)	135	198	-63
MnO_2–VGCF–Naf:PTFE	122	198	-76

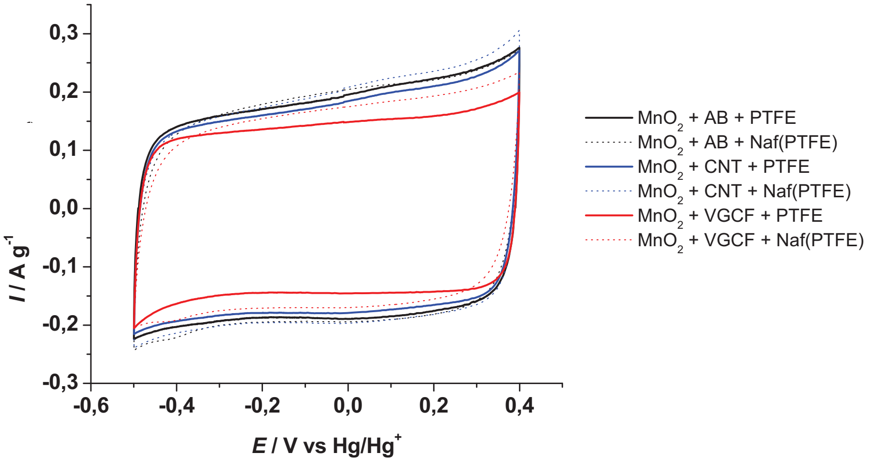

Figure 28: *Cyclic voltammograms of the studied electrodes based on MnO_2 ($\approx$ 25 mg) in a 0.65 M K_2SO_4 aqueous solution at a scan rate of 2 mV/s.*

6.2.5 Electrochemical characterization

Figure 28 presents cyclic voltammograms of different composite films ($m_{\mathrm{act}} = 25$ mg) in a 0.65 M K_2SO_4 aqueous solution. The featureless cyclic voltammograms indicate that the electrode is charged and discharged at a constant rate over the complete cycle. Moreover, the CV shows a mirror image with respect to the zero-current line and a rapid current response on voltage reversal at each end potential in agreement with literature data for this type of MnO_2 electrode material [20].

6.2.5.1 Effect of the MnO_2:carbon:binder ratio

In this section, the effect of the ratio of the different compounds of the composite electrode and the type of the binder polymer on the specific capacitance was investigated. The follow-

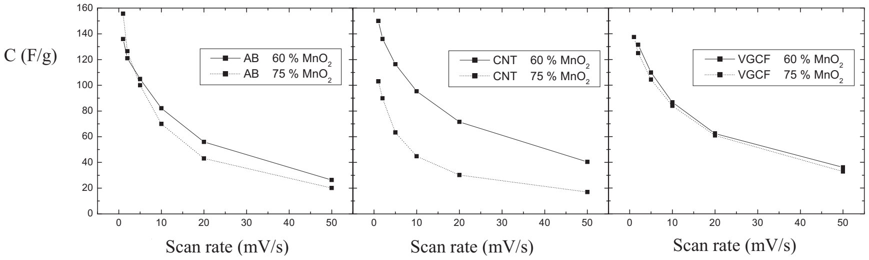

Figure 29: *Variation of the specific capacitance as function of scan rate for the three types of electrodes (active mass ∼15 mg) using different carbon additives.*

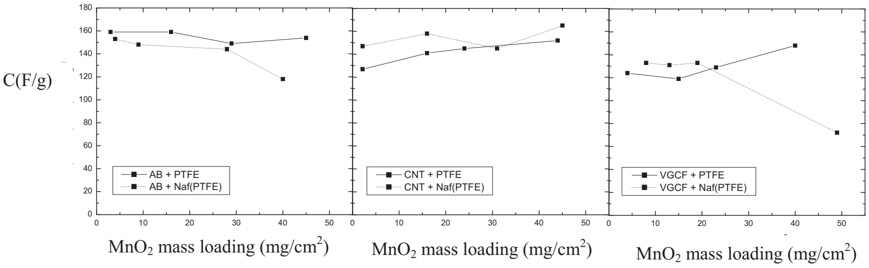

Figure 30: *Variation of the specific capacitance of composite electrode as function of MnO_2 mass loading (scan rate 2 mV/s)*

ing ratios were used: 60:30:10 MnO_2:carbon:binder, and 75:15:10 MnO_2:carbon:binder. The binder used in this study was solid PTFE. The specific capacitance was determinate from the cyclic voltammogram. Figure 29 shows the variation of the specific capacitance as a function of the scan rate for various electrodes. From the comparison between the three tested carbons, one can observe that the ratio does not affect the specific capacitance at low scan rate and the rate capability at high scan rate for the electrodes made with AB and VGCF as conducting additive. However, the specific capacitance of electrodes with CNTs decreases dramatically with the increase of the scan rate. From the results of Figure 29, the ratio 60:30:10 was used for the preparation of the composite electrodes for the remainder of the study.

6.2.6 Effect of MnO_2 loading on specific capacitance

Figure 30 shows that the MnO_2 loading does not significantly affect the specific capacitance of the composite electrodes containing AB and CNT even at high loading mass (45 mg/cm^2) when PTFE is used as the binder.

The composite electrodes show a specific capacitance around 160 F/g which in agreement with the previous report of Brousse and coworkers [59]. The electrode using CNT and Nafion shows the highest capacitance. For the electrodes with Nafion, electrodes containing AB and VGCF present a significant decrease of capacitance for the mass loading larger than 30 mg/cm^2. However, the electrodes containing PTFE maintain the specific capacitance for

Table 6: *Specific capacitance of MnO_2-based electrodes from this work and from the literature.*

MnO_2 loading (mg/cm^2)	C_{sp} (F/g)	Reference
Thin films		
0.001	678	[41]
0.018	330	[60]
0.116	150	[60]
0.045	353	[61]
0.13–0.15	285	[58]
0.18	243	[62]
0.22	230	[63]
0.20–0.25	220	[64]
0.47	260	[44]
4.70	50	[44]
Composites		
0.4	381	[65]
0.6	153	[65]
0.64	281	[66]
40	120	[59]
45	165	This study

the mass loading over than 40 mg/cm^2. The specific capacitance recorded in this work is 160 F/g for a MnO_2 loading of 45 mg/cm^2. This is one of highest capacitance for high loaded manganese oxide electrode ever reported in the open literature. Table 6 shows a comparison of results of this work with selected results from the literature.

6.2.7 Relationship between the pore texture and the electrochemical data

Table 7 correlates the values of the BET surface area, reported above in Table 5, together with the specific capacitance recorded at slow scan rate and for the thinnest films investigated. The capacitance values are taken from the data of Figure 30. These experimental conditions and electrodes were selected to establish the relationship between the BET surface area and the specific capacitance in order to avoid polarization and diffusion effects that could be observed at higher scan rates and for thicker film electrodes. It seems that a relatively good correlation can be established between the BET surface area and the specific capacitance with the exception of the MnO_2/CNT/Nafion electrode which yielded a much lower specific capacitance.

Table 7: *Pore texture and electrochemical data for various samples.*

Sample	Measured S_{BET} (m^2/g)	Calc'd S_{BET} (m^2/g)	Capacitance (F/g)
MnO_2	320		
CNT	280		
AB	86		
VGCF	21		
MnO_2–AB–PTFE(s)	190	218	160
MnO_2–AB–Naf:PTFE	175	218	154
MnO_2–CNT–PTFE(s)	230	276	128
MnO_2–CNT–Naf:PTFE	196	276	148
MnO_2–VGCF–PTFE(s)	135	198	123
MnO_2–VGCF–Naf:PTFE	122	198	132

One aim of this work was to improve the electronic conductivity of the composite electrodes by addition of various carbon conductors. The simple idea of using carbon conductive materials with different size and form has been tested. For example, VGCF which have lengths in the 10–20 μm range should improve the electrochemical accessibility (and capacitance) of the low conductivity manganese oxide relative to shorter carbon nanotubes (length=0.1–10 μm). Unfortunately, our capacitance measurements do not show that this is the case and on the contrary the specific capacitance decreased when the larger carbon particles are used to fabricate the composite electrode. In fact, the smallest AB particles (diameter=0.042 μm) enable to obtain the best performance. Similarly, Nafion was used as binder, instead of PTFE, to increase the ionic conductivity of the composite electrode materials due to the presence of sulfonated groups. In this case, it appears that contrary to the expectation, Nafion has a negative effect. This is believed to be due to the fact that Nafion blocks access to a fraction of the active surface of the manganese dioxide particles.

7 Project Conclusions and Key Results

1. The formation of titanium oxide nanotubes by anodization in an aqueous solution of $NH_4HF_2/NH_4H_2PO_4$ has led to an increase in the electrode surface, and the subsequent electrochemical reduction in acetonitrile solution has increased the conductivity of the electrode without losing the nanotube-like structure. It is necessary to note that even after electrochemical reduction the electric conductivity is still too low.

2. The deposition of carbon nanotubes on microfibrous carbon paper is a simple method to obtain a multiscaled carbon paper-carbon nanotubes (CP-CNT) substrate, which can be used as current collector and substrate in active material for electrochemical capacitors

3. The deposition of carbon nanotubes on a conducting substrate (stainless steel) by electrophoretic technique allows the formation of a CNTs film which is highly porous with open space between the entangled nanotubes. The SS-CNT substrate can be used as efficient current collector for electrode of electrochemical capacitors.

4. The development of mixed oxide RuMn has been reported and used as active material for electrode of electrochemical capacitors. The study of the effect of the composition of those electrodes showed that the highest capacitance where obtained with those containing 80% active material. However, this study demonstrated that the synthesis of RuO_2/MnO_2 active material using the co-precipitation method permit to obtain capacitive performances similar to those obtained for a simple mechanical mixing of RuO_2 and MnO_2 powders. These specific capacitance values are also similar to those expected by taking into account the specific capacitance of each single oxide and their fraction in the mixed oxide. The co-precipitation method used for RuO_2 and MnO_2 does not allow to obtain synergetic effect on specific capacitance and potential windows. When a titanium grid is used as current collector with RuO_2/MnO_2 composite electrodes specific capacitance results similar to those obtained with a stainless steel grid are obtained.

5. Low-cost nanocomposite materials based on a simple *in situ* coating technique of a multiscaled CNT/microfibrous CP substrate by manganese oxide were synthesized and studied for electrochemical capacitor applications. This composite is an efficient reducing agent of MnO_4^- to MnO_2 compared to microfibrous carbon. The specific capacitance of the CP-CNT-MnO_2 nanocomposite electrode is as high as 322 F/g compared to that of CP-MnO_2, which is 125 F/g. EIS shows that the addition of CNT improves electronic conductivity and the electrical contact between the active material and the current collector.

6. Novel cost-effective nanocomposite materials based on nanosized-manganese oxide and carbon nanotubes were synthesized by using the electrophoretic deposition (EPD) of CNTs on a stainless steel (SS) substrate followed by direct spontaneous reduction of MnO_4^- ions on the multi scaled SS-CNT substrate to form $MnO_2\cdot$ The specific capacitance of the SS-CNT-MnO_2 nanocomposite electrode is as high as 869 F/g and stable over long cycling.

7. Thin film $Ru_xMn_{1-x}O_2$ electrodes were prepared by thermal decomposition at 450°C of ruthenium and manganese salt mixed solutions deposited by paint brushing at the surface of a titanium substrate. The $Ru_{0.6}Mn_{0.4}O_2$ electrodes have been shown to have their highest specific capacitance in acidic electrolyte.

8. The best carbon additive for the preparation of MnO_2-based composite electrode was found to be acetylene black. More advanced materials such as carbon nanotubes and vapor grown carbon fibres do not appear to lead to an improvement of the capaci-

tance. Furthermore, using ionically conducting binder Nafion, does not improve the performance of the composite electrodes.

References

[1] Conway, B. E. (1999), Electrochemical Supercapacitors: Scientific Fundamentals and Technological Applications, Kluwer Academic/Plenum Press.

[2] Miller, J. (2007), A Brief History of Supercapacitors, *Batteries and Energy Storage Technology*, p. 61.

[3] Xiong, C. and Balkus, K. (2005), *J. Chem. Mater.*, 17, 5136.

[4] Wu, J. (2004), *J. Crystal Growth*, 269, 347.

[5] Wu, J., Huang, B., Wang, M., and Osaka, A. (2006), *J. Am. Ceram. Soc.*, 89, 2660.

[6] Kasuga, T., Hiramatsu, M., Hoson, A., Sekino, T., and Niihara, K. (1998), *Langmuir*, 14, 3160.

[7] Kasuga, T. (2006), *Thin Solid Films*, 496, 141.

[8] Gong, D., Grimes, C., Varghese, O., Hu, W., Singh, R., Chen, Z., and Dickey, E. (2001), *J. Mater. Res.*, 16, 3331.

[9] Li, H., Ba, X., Ling, Y., Li, J., Zhang, D., and Wang, J. (2006), *Electrochem. Solid-State Lett.*, 9, B28.

[10] Zhu, Y., Li, H., Koltypin, Y., Hacohen, Y., and Gedanken, A. (2001), *Chem. Commun.*, p. 2616.

[11] Chamoulaud, G. and Bélanger, D. (2007), Metal Oxide Materials and Collector Efficiency in Electrochemical Supercapacitors: First Annual Report, (CR 2007-233) Defence R&D Canada – Atlantic.

[12] Portet, C., Taberna, P., Simon, P., and Laberty-Robert, C. (2004), *Electrochim. Acta*, 49, 905.

[13] Portet, C., Taberna, P., Simon, P., and Flahaut, E. (2006), *J. Electrochem. Soc.*, 153, A649.

[14] Shaffer, M. S. P., Fan, X., and Windle, A. H. (1998), *Carbon*, 36, 1603.

[15] Thomas, B. J. C., Boccaccini, A., and Shaffer, M. S. P. (2005), *J. Am. Ceram. Soc.*, 88, 980.

[16] Pico, F., Ibanez, J., Centeno, T., Pecharroman, C., Rojas, R., Amarilla, J., and Rojo, J. (2006), *Electrochim. Acta*, 51, 4693.

[17] Burri, D., Choi, K., Han, D.-S., Koo, J.-B., and Park, S.-E. (2006), *Catalysis Today*, 115, 242.

[18] Sato, Y., Yomogida, K., Nanaumi, T., Kobayakawa, K., Ohsawa, Y., and Kawai, M. (2000), *Electrochem. Solid-State Lett.*, 3, 113.

[19] Zang, J., Jiang, D., B.Chen, Zhu, J., Jiang, L., and Fang, H. (2001), *J. Electrochem. Soc.*, 148, A1362.

[20] Lee, H. Y. and Goodenough, J. (1999), *J. Solid State Chem.*, 144, 200.

[21] Toupin, M., Brousse, T., and Bélanger, D. (2002), *Chem. Mater.*, 14, 3946.

[22] Zheng, J. (1999), *Electrochem. Solid State Lett.*, 2, 359.

[23] Brousse, T., Toupin, M., Dugas, R., Athouël, L., Crosnier, O., and Bélanger, D. (2006), *J. Electrochem. Soc.*, 153, A2171.

[24] Zheng, J. P. and Jow, T. R. (1995), *J. Electrochem. Soc.*, 142, L6.

[25] Zheng, J. P., Cygan, P. J., and Jow, T. R. (1995), *J. Electrochem. Soc.*, 142, 2699.

[26] Xie, X. and Gao, L. (2007), *Carbon*, 45, 2365.

[27] Toupin, M., Brousse, T., and Bélanger, D. (2004), *Chem. Mater.*, 16, 3184.

[28] Bélanger, D., Brousse, T., and Long, J. W. (2008), *Interface*, 17, 49.

[29] Devaraj, S. and Munichandraiah, N. (2005), *Electrochem. Solid-State Lett.*, 8, A373.

[30] Zhou, Y. K., He, B. L., Zhang, F. B., and Li, H. L. (2004), *J. Solid State Electrochem.*, 8, 482.

[31] Pinero, E. R., Khomenko, V., Frackowiak, E., and Béguin, F. (2005), *J. Electrochem. Soc.*, 152, A229.

[32] Wang, G. X., Zhang, B. L., Yu, Z. L., and Qu, M. Z. (2005), *Solid State Ionics*, 176, 1169.

[33] Subramanian, V., Zhu, H., and Wei, B. (2006), *Electrochem. Commun.*, 8, 827.

[34] Huang, X., Pan, C., and Huang, X. (2007), *Mater. Lett.*, 61, 934.

[35] Ma, S. B., Ahn, K. Y., Lee, E. S., Oh, K. H., and Kim, K. B. (2007), *Carbon*, 45, 375.

[36] Ma, S. B., Nam, K. W., Yoon, W. S., Yang, X. Q., Ahn, K. Y., Oh, K. H., and Kim, K. (2008), *J. Power Sources*, 178, 483.

[37] Wu, M., Snook, G. A., Chen, G. Z., and Fray, D. J. (2004), *Electrochem. Commun.*, 6, 499.

[38] de Levie, R. (1963), *Electrochim. Acta*, 8, 751.

[39] Keiser, H., Beccu, K. D., and Gutjahr, M. A. (1976), *Electrochim. Acta*, 21, 539.

[40] Macdonald, D. D., Urquidi-Macdonald, M., Bhakta, S. D., and Pound, B. G. (1991), *J. Electrochem. Soc.*, 138, 1359.

[41] Pang, S. C., Anderson, M. A., and Chapman, T. W. (2000), *J. Electrochem. Soc.*, 147, 444.

[42] Pang, S. C. and Anderson, M. A. (2000), *J. Mater. Res.*, 15, 2096.

[43] Chin, S. F., Pang, S. C., and Anderson, M. (2002), *J. Electrochem. Soc.*, 149, A379.

[44] Broughton, J. N. and Brett, M. J. (2004), *Electrochim. Acta*, 49, 4439.

[45] Bordjiba, T. and Bélanger, D. (2009), *J. Electrochem. Soc.*, 156, A378.

[46] Lee, C. Y., Tsai, H. M., Chuang, H., Li, S. Y., Lin, P., and Tseng, T. Y. (2005), *J. Electrochem. Soc.*, 152, A716.

[47] Fan, Z., Chen, J., Wang, M., Cui, K., Zhou, H., and Kuang, Y. (2006), *Diam. Relat. Mater.*, 15, 1478.

[48] Wu, M., Zhang, L., Gao, J., Zhou, Y., Zhang, S., and Chen, A. (2008), *J. Electrochem. Soc.*, 155, A355.

[49] Pandolfo, A. G. and Hollenkamp, A. F. (2006), *J. Power Sources*, 157, 11.

[50] Frackowiak, E. and Béguin, F. (2001), *Carbon*, 39, 937.

[51] Prasad, K. and Miura, N. (2004), *J. Power Sources*, 135, 354.

[52] Fischer, A. E., Pettigrew, K., Rolison, D. R., Stroud, R. M., and Long, J. (2007), *Nano. Lett.*, 7, 281.

[53] Lin, C.-K., Chuang, K.-H., Lin, C.-Y., Tsay, C.-Y., and Chen, C.-Y. (2007), *Surf. Coat. Tech.*, 202, 1272.

[54] JCPDS X-ray Diffraction Files 41-1442.

[55] JCPDS X-ray Diffraction Files 40-1290.

[56] JCPDS X-ray Diffraction Files 24-0735.

[57] Fernandez, J. L., de Chialvo, M. R. G., and Chialvo, A. C. (2002), *J. Appl. Electrochem.*, 32, 513.

[58] Hu, C. C. and Tsou, T. W. (4), *Electrochem. Commun.*, 2002, 105.

[59] Brousse, T., P.-L, Taberna, Crosnier, O., Dugas, R., Guillemet, P., Scudeller, Y., Zhou, Y., Favier, F., Bélanger, D., and Simon, P. (2007), *J. Power Sources*, 173, 633.

[60] Nam, K. and Kim, K. (2006), *J. Electrochem. Soc.*, 153, A81.

[61] Wei, J., Nagarajan, N., and Zhitomirsky, I. (2007), *J. Mater. Process. Technol.*, 186, 356.

[62] Wu, M. and Chiang, P. J. (2004), *Electrochem. Solid-State Lett.*, 7, A123.

[63] Hu, C. and Wang, C. (2003), *J. Electrochem. Soc.*, 150, A1079.

[64] Hu, C. and Tsou, T. (2003), *J. Power Sources*, 115, 179.

[65] Rios, E., Rosario, A., Mello, R., and Micaroni, L. (2007), *J. Power Sources*, 163, 1137.

[66] Sivakkumar, S., Ko, J. M., Kim, D. Y., Kim, B., and Wallace, G. (2007), *Electrochim. Acta*, 52, 7377.

Symbols and Abbreviations

C Capacitance

C_{sp} Specific capacitance

$C_{sp,E}$ Electrode specific capacitance

$C_{sp,M}$ Active material specific capacitance

$S_{\mathbf{BET}}$ BET surface area

$m_{\mathbf{act}}$ Active mass loading

AB Acetylene Black

BET Brunauer, Emett, and Teller method of measuring surface area

CNT Carbon nanotube

CP Carbon paper

CV Cyclic voltammetry or cyclic voltammogram

EDX Energy dispersive x-ray analysis

EIS Electrochemical impedance spectroscopy

EPD Electrophoretic deposition

ESR Equivalent series resistance

OCP Open circuit potential

PTFE Poly(tetrafluoroethylene)≡Teflon

SEM Scanning electron microscope, microscopy, or micrograph

SS Stainless steel

VGCF Vapour-grown carbon fibre

XRD X-ray diffraction

This page intentionally left blank.

Distribution list

DRDC Atlantic CR 2010-255

Internal distribution

2	Colin Cameron; 1 CD, 1 paper
1	Trisha Huber
1	Ed Andrukaitis
1	Royale Underhill, GL/MC
1	Leon Cheng, H/DL(A)
3	DRDC Atlantic Library

Total internal copies: 9

External distribution

2 Prof. Daniel Bélanger; 1 CD, 1 paper
Dept. de chimie
Université de Québec à Montréal
CP 888 Succ. Centre Ville
Montreal, QC H3C 3P8

1 Prof. Peter G. Pickup
Department of Chemistry
Memorial University of Newfoundland
St. John's NL A1B 3X7

1 Prof. Michael Freund
Department of Chemistry
University of Manitoba
Winnipeg, MB R3T 2N2

1 Prof. Alex Adronov
Department of Chemistry
McMaster University
1280 Main St. W
Hamilton, ON L8S 4M1

1 DRDKIM

1 Library and Archives Canada
Attn: Military Archivist, Government Records Branch

Total external copies: 7

Total copies: 16

DOCUMENT CONTROL DATA

(Security classification of title, body of abstract and indexing annotation must be entered when document is classified)

1. ORIGINATOR (The name and address of the organization preparing the document. Organizations for whom the document was prepared, e.g. Centre sponsoring a contractor's report, or tasking agency, are entered in section 8.)

Université du Québec à Montréal
Département de Chimie
Case postale 8888, Succ. Centre-ville
Montréal (Québec) H3C 3P8

2a. SECURITY CLASSIFICATION (Overall security classification of the document including special warning terms if applicable.)

UNCLASSIFIED

2b. CONTROLLED GOODS

(NON-CONTROLLED GOODS)
DMC A
REVIEW: GCEC JUNE 2010

3. TITLE (The complete document title as indicated on the title page. Its classification should be indicated by the appropriate abbreviation (S, C or U) in parentheses after the title.)

Metal Oxide Materials and Collector Efficiency in Electrochemical Supercapacitors: Final Report

4. AUTHORS (Last name, followed by initials – ranks, titles, etc. not to be used.)

Bordjiba, T.; Chamoulaud, G.; Médard, C.; Lechasseur, M. H.; Bélanger, D.

5. DATE OF PUBLICATION (Month and year of publication of document.)

December 2010

6a. NO. OF PAGES (Total containing information. Include Annexes, Appendices, etc.)

70

6b. NO. OF REFS (Total cited in document.)

66

7. DESCRIPTIVE NOTES (The category of the document, e.g. technical report, technical note or memorandum. If appropriate, enter the type of report, e.g. interim, progress, summary, annual or final. Give the inclusive dates when a specific reporting period is covered.)

Contract Report

8. SPONSORING ACTIVITY (The name of the department project office or laboratory sponsoring the research and development – include address.)

Defence R&D Canada – Atlantic
PO Box 1012, Dartmouth NS B2Y 3Z7, Canada

9a. PROJECT OR GRANT NO. (If appropriate, the applicable research and development project or grant number under which the document was written. Please specify whether project or grant.)

12sz07

9b. CONTRACT NO. (If appropriate, the applicable number under which the document was written.)

W7707-063348

10a. ORIGINATOR'S DOCUMENT NUMBER (The official document number by which the document is identified by the originating activity. This number must be unique to this document.)

DRDC Atlantic CR 2010-255

10b. OTHER DOCUMENT NO(s). (Any other numbers which may be assigned this document either by the originator or by the sponsor.)

11. DOCUMENT AVAILABILITY (Any limitations on further dissemination of the document, other than those imposed by security classification.)

(X) Unlimited distribution
( ) Defence departments and defence contractors; further distribution only as approved
( ) Defence departments and Canadian defence contractors; further distribution only as approved
( ) Government departments and agencies; further distribution only as approved
( ) Defence departments; further distribution only as approved
( ) Other (please specify):

12. DOCUMENT ANNOUNCEMENT (Any limitation to the bibliographic announcement of this document. This will normally correspond to the Document Availability (11). However, where further distribution (beyond the audience specified in (11)) is possible, a wider announcement audience may be selected.)

13. ABSTRACT (A brief and factual summary of the document. It may also appear elsewhere in the body of the document itself. It is highly desirable that the abstract of classified documents be unclassified. Each paragraph of the abstract shall begin with an indication of the security classification of the information in the paragraph (unless the document itself is unclassified) represented as (S), (C), or (U). It is not necessary to include here abstracts in both official languages unless the text is bilingual.)

The Supercapacitor Technology Investment Fund (TIF) project aimed to develop improved supercapacitor performance through the design of better electrode materials. This will ultimately yield devices with elevated power and energy densities and/or performance tailored to the needs of the Canadian military. This report deals with the development of electrochemical supercapacitors based on MnO_2 and binary manganese and ruthenium oxides with the use of various current collectors. The binary oxides were prepared and characterized by physicochemical and electrochemical techniques. The effect of the heat-treatment on the capacitance of the binary oxides was investigated as well as the effect of the supporting electrolyte, the current collector and the composition of the composite electrode. Carbon nanotubes were coated on a carbon paper and used as support for the binderless spontaneous formation of MnO_2. A correlation is drawn between pore size and capacitor performance for the combinations of active material, binder, and conductive carbon. New results are presented along with a summary of results from the previous two years of the project, and the performance of these new electrode materials is highlighted.

14. KEYWORDS, DESCRIPTORS or IDENTIFIERS (Technically meaningful terms or short phrases that characterize a document and could be helpful in cataloguing the document. They should be selected so that no security classification is required. Identifiers, such as equipment model designation, trade name, military project code name, geographic location may also be included. If possible keywords should be selected from a published thesaurus. e.g. Thesaurus of Engineering and Scientific Terms (TEST) and that thesaurus identified. If it is not possible to select indexing terms which are Unclassified, the classification of each should be indicated as with the title.)

supercapacitor; ruthenium; manganese; mixed oxide; carbon; nanotubes